



Università
Ca' Foscari
Venezia

Master's Degree
in Science and
Technology of Bio and
Nanomaterials

Final Thesis

**Ceramics and scaffolds of
porous and strengthened
hydroxyapatite for
biomedical applications**

Supervisor

Prof. Robert Carlyle Pullar

Assistant supervisor

Prof. Paula Saebra

Graduand

Anna Bertocco

Matriculation number: 870494

Academic Year

2022 / 2023

Abstract

Biomaterials have been widely used in tissue engineering applications at an increasing rate in the past few years. In particular, bone tissue engineering has emerged as one of the most indispensable approaches to address bone trauma and several problems/diseases, like osteoporosis, bone cancer and bone infections, that arose in the last decades due to the accelerated growth of human population and consecutive increase of life expectancy.

Hydroxyapatite (HAp), an inorganic mineral belonging to the calcium apatite family and having the chemical formula $\text{Ca}_{10}(\text{PO}_4)_6(\text{OH})_2$, has been widely used specifically in this field due to its ability to mimic the mineral composition of bones and teeth in vertebrates, its excellent physical, chemical, and biological properties and facile adaptable surface functionalization with other innumerable essential materials.

This work of thesis mainly focuses on the synthesis of pure HAp nanoparticles through a rapid sol-gel method and subsequently the production of several ceramics and scaffolds having different porosity and gradient of strength for biomedical applications. In particular the structure and composition of these products are analyzed through X-Ray Diffraction (XRD) and Scanning Electron Microscopy (SEM). The photocatalytic activity and mechanical stability of the scaffold structures were tested by monitoring the degradation of an organic dye (methylene blue) and performing uniaxial tests. The bioactivity and cytotoxicity of the samples were evaluated by immersion in Simulated Body Fluid (SBF) and performing the MTT assay on the MG-63 (osteoblast) cell line, respectively.

List of Contents

Introduction

1. Bone tissue: Structure and Composition

- 1.1. Cellular composition
- 1.2. Extracellular matrix
- 1.3. Structure of the bones
- 1.4. Bone remodeling and Regeneration processes
- 1.5. Connective tissue diseases

2. Connective tissue trauma and diseases

- 2.1. Bone fractures and therapeutic approaches
- 2.2. Bone cancer and therapeutic approaches
- 2.3. Bone infections and therapeutic approaches

3. Development of bone substitutes

- 3.1. Implant features of new bone substitutes
- 3.2. Ceramic-based scaffolds
- 3.3. Calcium phosphate-based scaffolds

Materials and Methods

4. Synthesis procedures and analysis methods

- 4.1. Rapid sol-gel synthesis of Hydroxyapatite Nanoparticles
 - 4.1.1. Hydroxyapatite powder from calcium nitrate tetrahydrate
 - 4.1.2. Hydroxyapatite powder from calcium acetate hydrate
- 4.2. Preparation of the porous ceramic materials
- 4.3. Preparation of the porous scaffolds
- 4.4. Characterization analysis
 - 4.4.1. X-ray diffraction

-
- 4.4.2. Scanning electron microscopy and Optical microscopy
 - 4.4.3. Specific surface area with BET method
 - 4.5. Biomineralization assay with simulated body fluid
 - 4.5.1. Simulated body fluid solution preparation
 - 4.5.2. Bioactivity of the scaffolds based on concentration
 - 4.5.3. SEM visualization of the immersed scaffolds
 - 4.6. Mechanical tests
 - 4.6.1. Measurement of the dimension of the scaffolds
 - 4.6.2. Testing machine
 - 4.7. Photocatalytic tests
 - 4.8. In vitro study: biocompatibility test
 - 4.8.1. MTT assay

Results and discussion

5. Characterization of the samples

- 5.1. X-Ray Diffraction
- 5.2. Scanning electron microscopy and Optical microscopy
- 5.3. Specific surface area
- 5.4. Bioactivity test: SEM visualization after SBF
- 5.5. Mechanical test
- 5.6. Photocatalytic test
- 5.7. In vitro study: biocompatibility test

Conclusions and Future works

Appendix A - Abbreviations

References

Acknowledgements

Introduction

1. Bones tissue: Structure and Composition

Bone tissue is a highly specialized form of connective tissue that consists of characteristic living bone cells (like osteoblasts and osteocytes) embedded in an extracellular matrix. The feature that distinguishes bones from other connective tissues is the mineralization of its matrix, which produces an extremely hard tissue capable of providing support and protection, allows locomotion and also serves as storage site for inorganic salts, in particular calcium and phosphate, that can be mobilized from the bone matrix and taken up by the blood in order to maintain appropriate levels in the bloodstream.¹

1.1. Cellular composition

The cells associated with bone tissue belong to five designated cell types: osteoprogenitor cells, osteoblast, osteocytes, bone-lining cells and osteoclasts (*Figure 1*). With the exception of the osteoclasts that are responsible for bone resorption, each of these cells may be regarded as a differentiated form of the same basic cell type, the mesenchymal stem cells present in the bone marrow.

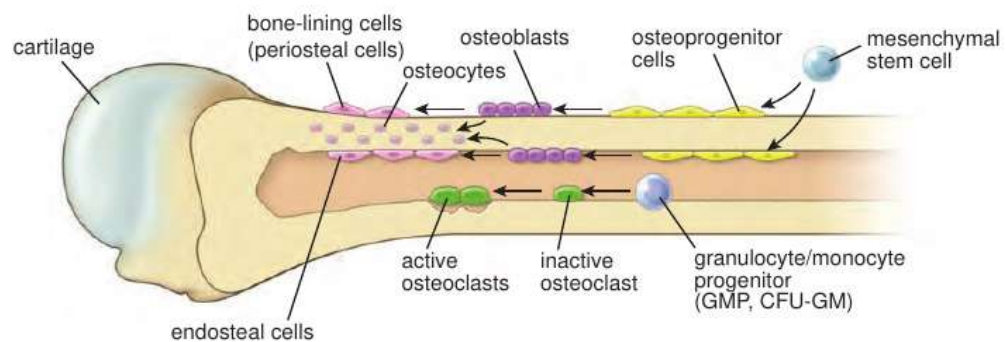


Figure 1: Schematic drawing of cells associated with bone

Osteoprogenitor cells derive directly from the process of differentiation of mesenchymal stem cells that is triggered by the presence of the transcription factor called core binding factor alpha-1 (CBFA1). They are located on the external and internal surfaces of bones and may also reside in the microvasculature supplying bone. In growing bones,

osteoprogenitor cells appear as flattened or squamous cells with lightly staining, elongate or ovoid nuclei and inconspicuous acidophilic or slightly basophilic cytoplasm. However, they also possess a rough-surfaced endoplasmic reticulum (rER), free ribosomes, a small Golgi apparatus and other organelles.¹ This specific morphology leads them to differentiate into a more active secretory cell, the osteoblast, when subjected to a stimulus.

Osteoblasts are versatile secretory cuboidal cells, representing 4-6% of the total resident cells in the bone, that possess the capacity of bone building and remodeling due to the fact that they retain the ability to divide and further differentiate into osteocytes or become bone-lining cells. Their morphologic characteristics include an abundant rough endoplasmic reticulum and prominent Golgi apparatus, as well as various secretory vesicles.² Since they can be classified as polarized cells, osteoblasts are responsible to secrete the mineralized organic bone matrix, known as osteoid, that is formed before the maturation of the bone tissue. This matrix, which contains a high amount of collagen (94%) and several proteins, growth factors and cytokines, allows the mineralization of the tissue.²

Osteocytes, which comprise 90-95% of the total amount of bone cells, are the most abundant and long-lived cells with a lifespan of up to 25 years.³ They are dendritic cells that are located with lacunae and formed when a subpopulation of osteoblasts become completely surrounded by the mineralized bone matrix at the end of a bone formation cycle. However, the morphology of the embedded osteocytes differs depending on the bone type, for example osteocytes from trabecular bone are more rounded than osteocytes from cortical bone, which display an elongated shape.² These cells are tightly connected to each other through gap junctions, forming a three-dimensional net buried in the bone matrix. These features allow them to have sensing and signal transport functions and they can act as mechanosensors, since their interconnected network has the capacity to detect mechanical pressures and loads, helping the adaptation of the bone to daily mechanical forces.⁴ Moreover, osteocyte apoptosis plays a key role in the bone resorption, acting as a chemotactic signal (during bone resorption, apoptotic osteocytes are engulfed by osteoclasts). In this way, osteocytes act as orchestrators of

bone remodeling, through regulation of osteoblast and osteoclast activities, and such ability helps to maintain calcium homeostasis.⁵

Bone lining cells (BLC's) are flat and elongated cells with attenuated cytoplasm, and a lack of organelles beyond the perinuclear region that cover inactive (non-modeling) bone surfaces in the mature/adult skeleton and are linked to each other or to osteocytes through gap junctions.² Regarding their origin, it is thought that they derive from previously active osteoblasts that have entered a quiescent phase. In fact, BLC's can differentiate into osteoblasts able to produce osteoid and the matrix vesicles responsible for the mineralization process, in the bone formation cycle.⁶ Though not completely understood, it is thought that these cells hamper the direct interaction between osteoclasts and bone matrix when bone resorption is not supposed to happen and participate in osteoclasts differentiation. Furthermore, it seems that they also have an important role in the maintenance and nutritional support of the osteocytes embedded in the underlying bone matrix and regulate the movement of calcium and phosphate into and out of the bone.¹

Osteoclasts are large, multinucleated cells with a marked acidophilia that are responsible for the bone resorption during the bone remodeling process. They derive from the fusion of mononuclear hematopoietic stem cells, in particular from the granulocyte and monocyte-macrophage lineage, and they become differentiated when stimulated by two essential factors: the monocyte/macrophage colony stimulating factor (M-CSF) and receptor activation of NF-kB ligand (RANKL), which is present on the surface of the stromal cells located in bone marrow (*Figure 2*).⁷ Once a mature osteoclast becomes active, it releases protons and lysosomal hydrolase enzymes into the constricted microenvironment of the extracellular space. In this way, the acidic environment initiates the degradation of the mineral component of the bone to calcium ions, soluble inorganic phosphates and water.¹ The correct balance between bone formation and destruction is essential to form an adequate bone mass so it is important to maintain the correct equilibrium between the activity of osteoblasts and osteoclasts. This is achieved not only by systemic factors but also by keeping a cross-talk between osteoblasts and osteoclasts. In this way, osteoclasts can produce factors that stimulate osteoblasts differentiation and function.

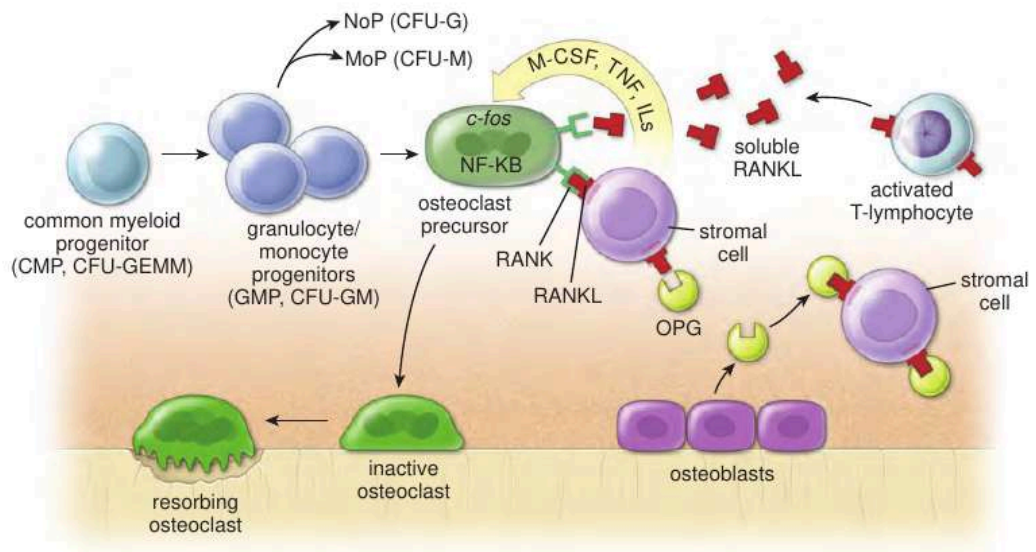


Figure 2: Graphic representation of the origin of osteoclasts

1.2. Extracellular matrix

The extracellular matrix (ECM) of each tissue is formed by the secreted product of resident cells of that tissue and organ, being composed by a mixture of structural and functional proteins arranged in a three-dimensional ultra-structure. The ECM is able not only to bind the cells together, but also, to influence their survival, development, shape and migratory behavior. Approximately 25% of the acellular component of bone consists of organic matter, while roughly 65% of the weight of dehydrated bone tissue is attributed to the inorganic phase.⁸ The organic matrix is formed essentially by type I collagen fibers (90%) immersed in a fundamental substance of bone, called ground substance, formed by different non-collagenous proteins including proteoglycans macromolecules, multiadhesive glycoproteins like osteonectin, osteopontin, bone sialoprotein I and II, bone-specific vitamin K-dependent proteins like osteocalcin (OCN), growth factors such as bone morphogenetic proteins (BMPs), and other minor proteins.⁹ While the inorganic matrix of the bone is composed mainly by hydroxyapatite needle-like crystals $[\text{Ca}_{10}(\text{PO}_4)_6(\text{OH})_2]$, being in the form of calcium salts, there are also smaller quantities of carbonate apatite and fluorapatite. These two types of matrices are responsible for the characteristic stiffness and resistance of bone tissue, since the

collagen and the non-collagenous matrix proteins form a scaffold for hydroxyapatite deposition, which hardens this connective tissue.¹⁰

1.3. Structure of the bones

The adult skeleton is composed of 80% cortical (compact) bone and 20% trabecular (cancellous or spongy) bone. These two forms of bone tissue have the same composition and structure, but differ in terms of density, porosity and location in the skeleton. The cortical bone comprises the outer tubular shell of the long bones and the outer surface of the small and flat bones, whereas the trabecular bone occurs near the ends of long bones, in the interior of small bones and between the surface of flat bones (*Figure 3*).¹ In addition, the cortical bone is harder, denser and has less porosity than the cancellous bone and it surrounds the bone marrow and the cancellous bone plates. Its fundamental functional units are the osteons, also known as the Haversian system, that have a cylindrical shape and form a network with several branches from which blood vessels run, allowing nutrient diffusion within the bone.¹¹ Regarding the trabecular bone, it is characterized by an interconnected network of small bone trabeculae that are aligned in the direction of the loading stress. This form of bone has a porosity of 40-95%, where these pores are filled with bone marrow and cells. Due to this high porosity, the trabecular bone provides less mechanical support when compared with cortical bone.^{12,13} Given the structure of the trabecular bone with larger surface area exposed to the bone marrow, and since bone resorption and formation occurs on the bones surface, it displays higher metabolic activity than the cortical bone. As a consequence, it is possible to assume that the cortical bone provides the mechanical and protective functions of the bone, whereas the cancellous bone provides its metabolic function and it is crucial for transmitting loads from the joint surface to the cortex.

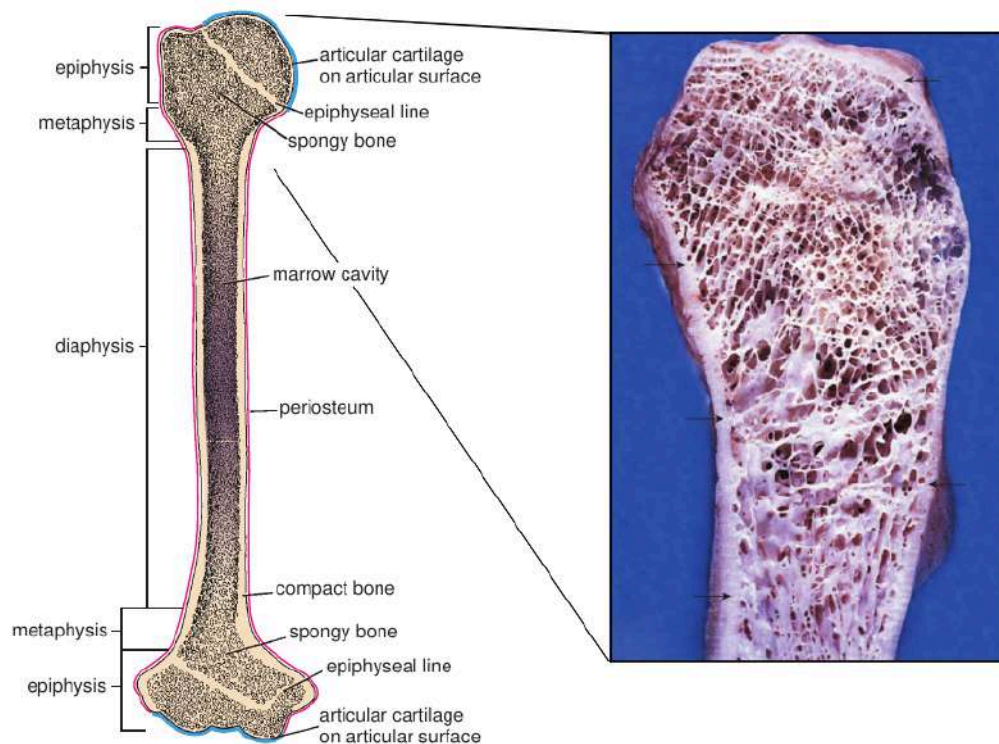


Figure 3: Structure of a typical long bone and longitudinal section of the epiphysis

Moreover, based on the arrangement of the collagen fibers, the bone tissue can be classified as immature bone or mature bone. The immature bone, also referred as bundle bone or woven bone, is characterized by a random arrangement of the collagen fibers and bone cells, and by not having an organized lamellated appearance it confers poor mechanical resistance to the tissue (*Figure 4a*).¹ Due to the fact that immature bone forms more rapidly than the mature ones, it is the major bone type in the process of developing the fetus and it is the first to be laid down both during the development and in the healing processes. On the other hand, the mature bone, also referred as lamellar bone, is largely composed of cylindrical units called osteons, that consist of concentric lamellae of bone matrix surrounding a central canal, called the Harvesian canal, which contains the vascular and nerve supply of the osteon (*Figure 4b*).^{1,11}

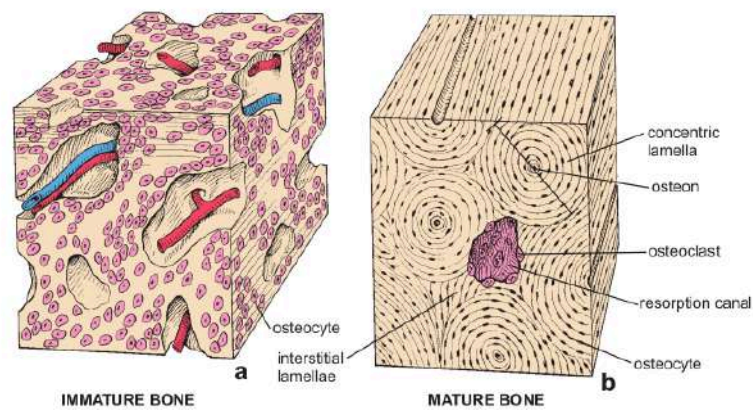


Figure 4: Diagram of immature bone (left) and mature bone (right)

In the lamellar tissue there are also the Volkmann canals, that are vascular connections that run perpendicularly with respect to the Haversian canals. The structural framework of the bone is completed by the presence of lacunae, small cavities present in the mineral matrix that contain osteocytes. Small channels (canaliculi) radiate from the lacunae to the osteonic (Haversian) canal to provide passageways through the hard matrix in order to connect the nearby lacunae, belonging both to the same lamella or to contiguous lamellae.^{1,9} The lamellae and canaliculi constitute a continuous system of branched cavities inside the bone that allows the metabolic and gaseous exchanges between the blood and the cells (Figure 5).

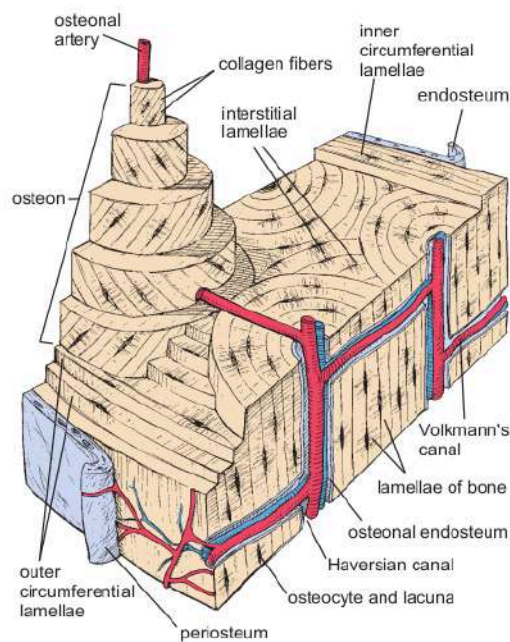


Figure 5: Diagram of a section of compact bone removed from shaft of a long bone

The formation of bones is called ossification and it occurs by two processes which differ according to the fact of whether a cartilage model serves as precursor for the formation of long bones (endochondral ossification), or whether the connective tissue, such as mesenchyme tissue, is used as a precursor for the formation of mainly the flat bones (intramembranous ossification) .

1.4. Bone remodeling and regeneration processes

Bone is a dynamic tissue that is continuously renewed through an active and dynamic process called bone remodeling, in which mature bone tissue is removed from the skeleton and is replaced by new tissue in order to maintain a constant bone mass. This lifelong process is performed by clusters of bone-resorbing osteoclasts and bone-forming osteoblasts, arranged within temporary anatomical structures known as “basic multicellular units” (BMUs), and the combined action of osteoclasts and bone living cells.¹⁴

The activity of these cells, including their formation, proliferation and differentiation, is regulated by local and systemic factors. The local factors include autocrine and paracrine

molecules such as growth factors and cytokines, produced by the bone cells and bone matrix factors released during bone resorption. The systemic factors include the parathyroid hormone (PTH), calcitonin, 1,25-dihydroxyvitaminD3 (calcitriol), glucocorticoids, androgens and estrogens.²

The remodeling cycle consists of five consecutive phases: activation, resorption, reversal, formation and termination. During the activation phase, osteocytes detect different inputs (such as micro-fractures or an alteration of the mechanical loading), or some signal molecules released in the bone microenvironment (such as IGFI, tumor necrosis factor- α , PTH and interleukin-6), which can lead to the activation of the lining cells and fuse together, in the presence also of the pre-osteoclasts, promoting the differentiation toward multinucleated osteoclasts.¹⁵

Afterwards, in the resorption phase, there is the recruitment of the osteoclast precursors to the remodeling site, performed by the osteoblasts, that adhere to the bone surface and start to dissolve bone, after being differentiated. After performing their function, osteoclasts undergo apoptosis in order to avoid an excessive bone resorption.¹⁵

The reversal phase is performed by reversal cells that are macrophage-like cells able to remove the debris produced during the degradation of the matrix, such as the undigested demineralized collagen matrix. Immediately afterwards, these reversal cells prepare the bone surface for the upcoming bone formation, which is mediated by osteoblasts.^{2,15}

In the formation phase, during the bone matrix resorption, there is a release of several growth factors (like BMPs, fibroblast growth factors and transforming growth factor- β) that are responsible for the recruitment of the osteoblasts in the resorbed area. After their recruitment, they begin to secrete collagen proteins (mainly type I collagen), non-collagenous proteins and proteoglycans, producing a newly formed bone matrix. In the initial stages, the osteoid is not calcified but later the osteoblasts are able to promote its mineralization through the synthesis of hydroxyapatite crystals.¹⁶

Finally, the termination phase takes place when the amount of resorbed bone has been completely replaced, which indicates the easing of bone formation. After mineralization, mature osteoblasts undergo apoptosis by reverting into the phenotype of bone lining cells or becoming osteocytes once embedded in the mineralized matrix. This indicates

that the bone surface has returned to a resting stage that will be maintained until the next cycle of remodeling is initiated.¹⁵

Another important feature of the bone is its intrinsic capacity for regeneration as part of the repair process in response to injury, as well as during skeletal development or continuous remodeling throughout adult life. This complex processes is comprised of a well-orchestrated series of biological events of bone induction and conduction, involving a number of cell types and intracellular and extracellular molecular signaling pathways, that happen within a well-define temporal and spatial sequence in order to optimize the repair of the skeleton, and also restore its functions.¹⁷ This process is involved in fracture healing, defects created by trauma, infection, tumor resection, congenital abnormalities and impaired or insufficient regeneration. From a clinical point of view, the majority of bone injuries, such as fractures, can heal without the formation of scar tissue and with its pre-existing properties largely restored. In addition, the newly formed bone is indistinguishable from the surrounding uninjured bone.¹⁸ The time required for the bone healing process depends directly on the type of fracture that has been undergone by the bone involved. In the case of a closed non-displaced fracture, bone healing is more rapid due to the fact that the broken bone maintains its original alignment. Meanwhile, the process of regeneration will require more time, and even surgical intervention in the case of open or displaced fractures, in which the bone breaks in two or more pieces moving out of alignment and eventually tearing the skin. However, both of these cases can lead to fracture healing in which bone regeneration is impaired, maybe due to inadequate immobilization, failed surgical intervention, insufficient biological response or infection. In addition, there are other conditions in which bone regeneration seems necessary in large quantities that is beyond the normal potential for self-healing.¹⁹ An example could be skeletal reconstruction of large bone defects created by trauma, infection, tumor resection and skeletal abnormalities, or cases in which the regenerative process is compromised, including avascular necrosis and osteoporosis. For these reasons, there are several bone regeneration and repair strategies to enhance surgical reconstructive procedures, including the use of alloplastic and allogenic materials, distraction osteogenesis, osteoconductive scaffolds and bone morphogenetic proteins (BMPs).

2. Connective tissue trauma and diseases

As previously explained, bone tissue is a particular connective tissue that is distinguished by its hardness and its characteristics of resistance to compression, traction and torsion. These properties are due to the presence of large quantities of crystals of mineral salts, which allow bone tissue to perform the typical structural and supporting functions. However, those functions can be compromised over time with the appearance of different common bone diseases, like bone cancer, osteoporosis and osteoarthritis, or severe internal and superficial trauma, like bone fractures and contusions.

2.1. Bone fractures and therapeutic approaches

A broken bone or a bone fracture occurs when a force exerted against a bone exceeds the resistance limits of the bone itself. The severity of the bone fracture depends on many factors, for example the strength and direction in which the external force is applied, what type of bone is particularly involved, the age of the patient and their general health. However, bone fractures may be the result of traumatic incidents, like sports injuries, vehicle accidents and falls, and conditions such as osteoporosis and some types of cancer that cause bones to crack easily.²⁰

Osteoporosis, which literally means porous bone, is a disorder characterized by progressive loss of normal bone strength and density accompanied by the deterioration of its microarchitecture, which it is caused by an imbalance between osteoclast-mediated bone resorption and osteoblast-mediated bone deposition, resulting in decreased bone mass, enhanced bone fragility, and increased risk of fracture (*Figure 6*). Femoral head and neck fractures (also known as hip fractures), wrist fractures and compressive vertebrae fractures are common injuries that frequently disable elderly people and can even lead them to a premature death due to the possible complication of hospitalization. For these reasons, osteoporosis has emerged as the most common and prevalent bone disorder worldwide (75 million people in the US, Europe and Japan), being the major cause of disability in older people and it can even lead to a premature death in these individuals due to the possible complication of hospitalization.¹

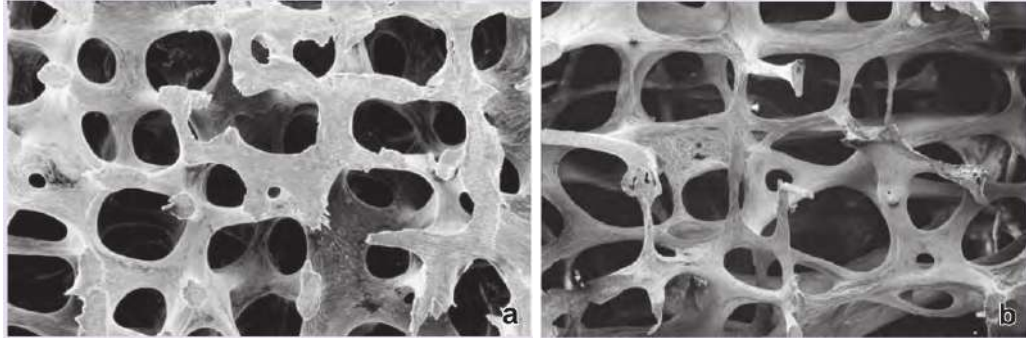


Figure 6: Scanning electron micrograph of trabecular bone obtained from a healthy individual (a) and from an elderly woman with extensive signs of osteoporosis (b)

The repair of bone fractures is a regenerative process that requires many of the biological events of embryonic skeletal development and it frequently leads to the successful healing and recovery of the damaged bone, but about 5-10% of fractures can lead to a delayed healing or non-union.²¹ Traditional treatments for patients with osteoporosis include an improved diet with vitamin D and calcium supplementation alongside moderate exercise in order to further decrease the loss of bone mass.¹ In addition to diet and exercise, pharmacologic therapy is usually employed with either antiresorptive medications, which primarily decrease the rate of bone resorption, or anabolic medications, which tend to increase bone formation (promote osteogenesis).²² However, if the bone damage is particularly severe, it is necessary to apply more invasive clinical approaches that include distraction osteogenesis and bone transport, and the use of different bone-grafting methods, like autologous bone grafts (autografts), allografts and synthetic bone grafts (ceramic materials such as calcium phosphates, Bioglass and calcium sulfate). Moreover, there are also non-invasive methods of biophysical stimulation, such as low-intensity pulsed ultrasound (LIPUS), capacitively coupled electrical field (CCEF) and pulsed electromagnetic fields (PEMF), that can be used as adjuncts to enhance bone regeneration.²³ In any case, the “gold-standard” treatment is autologous bone grafting, where several bone sites can be used for bone-graft harvesting. The anterior and posterior iliac crests of the pelvis are the most commonly used donor sites, since they present all the required elements for bone healing: osteoinduction (BMPs and other growth factors), osteogenesis (osteoprogenitor cells) and osteoconduction (bioactive chemicals within the scaffold).¹⁷

Despite all the advanced achievements obtained in recent decades, there are still many drawbacks in the use of bone grafts. The use of autografts can be limited by the volume of the bone that is possible to harvest. Furthermore, the transplanted autograft may lead to complications due to defect size, reduced mobility at the harvest site, generation of local hematoma and remodeling issues of the implanted bone.²⁴ The application of allografts, which have been harvested from other individuals of the same species (cadavers) can be hampered by bone tissue integration from the host and vascularization tissues. Regarding distraction osteogenesis, it can be a painful process due to the fact that new bone is regenerated as a result of gradually separating two viable osteotomized bone edges. In particular, during the "distraction phase", it is necessary to apply a pain-inducing force in order to overcome the resistance of soft tissue (such as skin) and maintain the separation of the bone edges. In addition, this technique is also associated with poor healing and re-fracture. Consequently, there is the need to develop novel long term treatments and therapies with respect to the standard method currently used for bone regeneration. To this extent, bone graft substitutes (BGS) may be the "best" answer to help impaired fracture healing.²¹

2.2. Bone cancer and therapeutic approaches

The three most common forms of primary bone cancers are osteosarcoma (OS), the Ewing sarcoma family of tumors, and chondrosarcoma, osteosarcoma being the most common among them. Osteosarcoma has a worldwide incidence of one to three cases annually per million individuals and is the most common primary malignant bone sarcoma with a bimodal age distribution. The highest incidence is in children and adolescents (between the ages of 10 and 25), with a second smaller peak of incidence in elderly individuals over 60 years.²⁵ It is characterized by the production of osteoid matrix by the malignant cells, and can arise mainly in the juxta-epiphyseal regions of long bones, such as the distal femur, the proximal tibia and the proximal humerus, close to the growth plate in the bone metaphysis, and less frequently in the skull, jaw, and pelvis.²⁶ This highly aggressive tumor typically arises in the medullary cavity of bone and progresses in order to destroy the cortical bone and the surrounding soft tissues, before extending and causing early systemic metastases (with a high probability of tumor

necrosis).²⁷ In terms of clinical approaches, the treatments currently used for this type of cancer includes preoperative (neoadjuvant) chemotherapy followed by surgical removal of all detectable disease (including metastases) and postoperative (adjuvant) chemotherapy. Radiation therapy is another treatment option as a local treatment of unresectable tumors, despite osteosarcoma being considered to be resistant to the application of radiation doses.²⁶

Ewing sarcoma is a small round blue cell malignancy that comprises 5-10% of the primary bone tumors, and is the second most common tumor that occurs predominantly in children or adolescents and young adults.²⁸ The most common sites for this cancer are the diaphysis or metaphysis region of long tubular bones, like the femur, but it can also arise from the pelvic bone and ribs. The other less-frequent and rare locations are in skull bones, the vertebra, the scapula and the small bones of hands and feet. Ewing sarcoma treatment includes at first cycles of neoadjuvant multi-agent chemotherapy to eradicate systemic disease and facilitate effective local control measures, with timely incorporation of radiation or surgical therapy and further adjuvant chemotherapy to prevent recurrence.²⁹

Chondrosarcoma is a rare malignant mesenchymal tumor, arising from several differentiated cells that produce chondroid matrices, that occurs mostly in adults over the age of 40.³⁰ Regarding the treatment, surgical resection is the primary and preferred type of treatment for patients with localized disease, whereas radiation therapy is mostly used for treating surgically hard-to-access sites and in palliation of local symptoms, requiring relatively high doses to cure it. Chemotherapy has been considered ineffective due to the relatively slow growth, low mitotic division and poor vascularity of the tumor that restricts drug penetration.³¹

Taking all this into consideration, it is possible to conclude that surgery, chemotherapy and radiation therapy are the main approaches for treating bone cancers. These therapies present some drawbacks that need to be taken in consideration: the short- and long-term collateral toxic effects of using chemotherapy, and even the possibility of inducing chemotherapeutic agent resistance, particularly in the case of osteoblastomas. In the case of radiation therapy, this modality is less frequently used given the potential side-effects of this approach, like the appearance of secondary malignancies and adverse

effects on bone growth. For these reasons it is necessary to find novel therapeutic modalities and more target-selective treatments for bone cancers.

2.3. Bone infections and therapeutic approaches

Bone defects may occur due to several congenital bone diseases or acquired conditions. Congenital bone abnormalities usually arise due to the absence or maldevelopment of bones, both caused by an altered homeostasis of the mineralization process, whereas acquired bone defects often appear because of a trauma, infection, cancer or even surgical resection. Some osteodegenerative conditions can be also responsible for bone loss over time, causing another type of bone defect.³² In particular, osteoarthritis, which is the inflammatory state that arises due to a progressive deterioration of the cartilaginous layer that covers the joint surfaces, can lead to the formation of osteophytes (or bone spurs). The reconstruction of bone defects is still a considerable clinical challenge, especially in the case of infections. It is often associated with abnormal bone remodeling due to a massive bone destruction and repair process at the site of infection, in response to bacteria and bacterial toxins. Unfortunately, this phenomenon is not unusual since the region of the defective bone and most of the synthetic bone substitutes are prone to bacterial adherence and subsequent biofilm formation, which in turn fosters the progression of the infection.³³ Some of the patients that undergo orthopedic surgeries suffer from postoperative deep infections after bone tumor surgeries and additional surgery is usually required. Furthermore, the administration of antibiotics for extended periods of time can also foster the infection due to the development of bacterial resistance. Trauma surgeries can also cause an infection after fracture fixation (IAFF) that can lead to non-union, delayed healing, permanent functional loss and even amputation of the affected limb. This kind of infection can happen with greater extension in open fractures, resulting in a particularly prolonged hospitalization and increased economic burden for patients or the state.³⁴ Therefore, the main goals of treating IAFF turn out to be the consolidation of the fracture, the eradication or, in some cases, the suppression of infection, the healing of the soft tissue envelope and the restoration of bone functionality. It is important to consider that sometimes the primary objective can be the healing of the bone compared to the treatment of the infection, since the internal

fixation device can be retrieved after the fracture consolidation, which results in eliminating the bacterial biofilm. In some cases, a suppressive therapy can be established with oral and intravenous antibiotics and the material must be retrieved after this treatment in order to avoid risk of recurrence of infection or chronic osteomyelitis.^{34,35} This is a progressive infection that results in an inflammatory destruction, necrosis and bone neof ormation, that can progress to a chronic and persistent stage with the possibility of being a lifetime chronic disease. Although there are surgical techniques to be applied to treat this condition (such as muscle grafts and antibiotic bone cements), bone infections are still a challenge. Therefore, it is necessary to improve both prevention and the current types of treatment available in order to achieve better patient care. Such improvements may be an increased bioavailability of medical devices consisting of porous materials capable of adsorbing antibiotics (functionalized antibacterial implants) or functionalized implants with antimicrobial peptides (AMPs), since they do not induce resistance within pathogens after exposure.³⁶

3. Development of bone substitutes

Bone injuries are very common and can cause serious changes in the quality of life of the patients. They can limit the ability to accomplish basic tasks, such as walking, and may also cause social and psychological problems. The current solutions available for these problems are essentially the use of bone graft transplants (autologous, allogeneic and xenogenic), bone transport methods and implants based on different types of materials. These types of intervention are needed in order to ensure the regeneration of the bone tissue and the complete restoration of its functions.³⁷ However, when bones are not able to restore themselves, bone tissue engineering shows a great therapeutic potential, since the challenge associated with the current orthopedic solutions can be solved by the development of suitable osteobiological materials.³⁸ These should replace the conventional allografts, autografts and xenografts, serving as implantable materials for bone substitutes, bone repair or remodeling. The biomaterials used can be classified into different types based on their chemical nature such as metal-based, ceramic-based, polymer-based or biological-based materials and composites, meaning for the latter a physical association between different materials.³⁹ Some materials can

even contain several bioactive molecules, including growth factors, that are normally expressed during bone regeneration.³⁸

Taking all of these aspects into consideration, the research of an implantable biomaterial that combines both functions of therapy and regeneration appears to be very promising for diseased and damaged bones.

3.1. Implant features of new bone substitutes

A good bone graft substitute should have high biocompatibility, low immunogenicity and it should be capable of molding itself according to the injured tissue needs. In the field of bone tissue engineering, porous and bioresorbable scaffolds are very important, since they are biocompatible 3D structures stimulated by several growth factors that help the migration, attachment, proliferation and differentiation of osteogenic cells, promoting the formation and regeneration of new bone tissue. In other words, a scaffold is able to mimic the functions and the properties, in terms of mechanical support, cellular activity and protein production, of natural bone.⁴⁰ It should possess the following characteristics: good bioactivity, biodegradability, biocompatibility and predictable rate of degradation; suitable porous structure to promote cell proliferation, vascular ingrowth and nutrient transportation; suitable surface morphology and physio-chemical properties to encourage intracellular signaling; and customized shape to adapt specific damaged bone.⁴¹ Biocompatibility is an important requirement, since this feature allows the material to establish a favorable interaction with the surrounding biological systems and eliciting minimal to mild tissue responses. Regarding biodegradability, this is a vital attribute for bone substitute scaffolds, since they can act as a supportive and temporary template for cell attachment and subsequent tissue development. In this way, cells have time to produce their extracellular matrix and eventually replace the scaffold. In addition, they can also be osteoconductive, osteoinductive and osseo-integrative in order to heal a possible damaged bone (*Figure 7*). Another important feature for the development of new bone substitutes, can be their capability of preventing bacterial infection, due to the current challenges associated with their treatments.

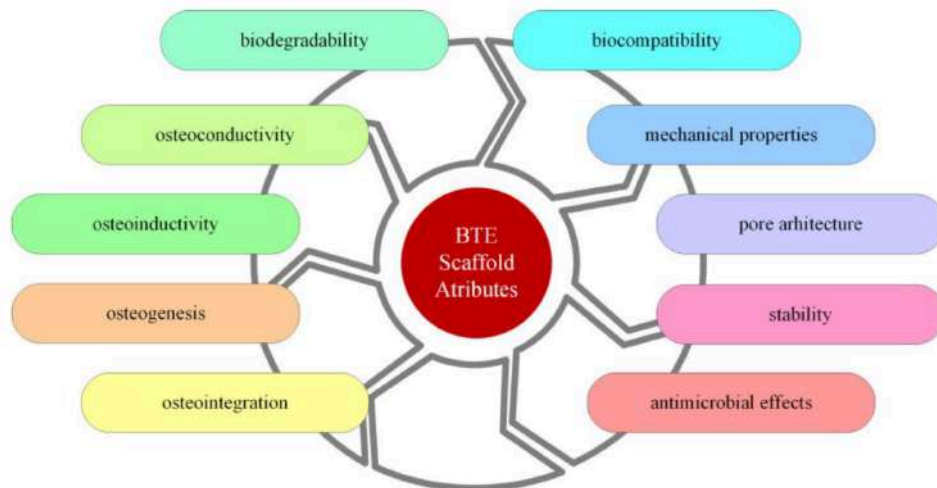


Figure 7: Schematic representation of the important features of a scaffold

3.2. Ceramic-based scaffolds

Ceramic based scaffolds are inorganic compounds being described as a family of materials with a wide variety of porosity, composition and structure, that are obtained by various manufacturing techniques. They have high stiffness and bioactivity, allowing them to act as a temporary framework to provide a suitable environment for cell adhesion and growth, and to promote bone tissue regeneration. Within this class of materials, there is also the group of bioceramics that possess specific biological or physiological functions, which allows them to be used directly in the human body. Bioceramic materials can be divided into three different categories: bioinert, bioactive and resorbable ceramics, which are actively involved in various metabolic processes.⁴⁰ The main differences between the first two types of ceramic rely on the fact that bioinert ceramics have a high mechanical strength, excellent biocompatibility and chemical stability. For this reason, a bioinert implement does not interact with the living tissue after implantation, meaning that it will not cause a reaction with the host. Bioactive ceramics are biodegradable and osteoconductive, which means that they are able to form direct bonds with the bone tissue and the surrounding soft tissues.⁴² In this way, both types of materials can be used as two integral parts of bone tissue engineering. Different types of ceramic-based materials can be used to produce scaffolds. Regarding bioinert ceramics, the most used materials are alumina (Al_2O_3), titanium dioxide (TiO_2 , also known as titania), zirconium

dioxide (ZrO_2 , also known as zirconia), hard porcelain and cordierite (a magnesium iron aluminum cyclosilicate). A commonly used bioactive ceramics is tricalcium phosphate (TCP), which has two structures with different atomic arrangements such as α -TCP and β -TCP.⁴³ This later has been more studied for bone applications, since pure α -TCP has a quick resorption rate that is faster than the formation of bone, limiting its use in biomedical applications. The class of bioceramics also includes calcium sulfate ($CaSO_4$), hydroxyapatite (HA pr HAp), akermanite containing calcium, silicon and magnesium, diopside ($MgCaSi_2O_6$) and bioglasses (BGs), often composed of Na_2O , CaO , SiO_2 and P_2O_5 .⁴⁴

3.3. Calcium phosphate-based scaffolds

Among the class of ceramic materials for biomedical applications and in particular for bone scaffolds, calcium phosphate (CaP) ceramics are the most widely used. They are minerals composed of calcium cations and phosphate anions that are known to be the major inorganic material in all native human bones (approximately 60%).⁴⁵ Besides that, calcium phosphate ceramics are known to be biocompatible, osteoconductive and osteoinductive, which makes them an important asset for bone regeneration. Furthermore, they have a high affinity for adhesion proteins and growth factors, such as bone morphogenetic protein-2 (BMP-2), which stimulates the proliferation and differentiation of osteoprogenitor cells, without the modification of their chemical surface.⁴⁶ However, the use of additives or surface coatings in CaP scaffolds can change their properties in order to enhance the processes of angiogenesis and osteogenesis. Bone cements, scaffolds, implants and coating techniques are some of the bone applications that use calcium phosphate ceramics. It is important to choose the type of calcium phosphate that best fits the desired application, since the osteoconductivity and osteoinductivity of CaP depends on its physical and chemical characteristics. Depending on the ratio of Ca/P, the temperature, the presence of water and impurities, calcium phosphate can crystallize in two forms: hydroxyphosphate of calcium, also known as hydroxyapatite (HA), and β -tricalcium phosphate.⁴⁷ In particular, hydroxyapatite is usually formed in the presence of a humid environment and a temperature lower than 900 °C, while β -tricalcium phosphate is more easily obtained in a dry environment and in the

presence of higher temperatures. Both forms are highly biocompatible and able to form direct bonds with hard tissues in a short period of time. For this reason, they are widely used as starting material for endo-osseous implants and coating materials for metal or polymeric prostheses. From a chemical point of view, hydroxyapatite is a naturally occurring mineral form of calcium apatite with the chemical formula $\text{Ca}_{10}(\text{PO}_4)_6(\text{OH})_2$, which crystallizes in the hexagonal system (*Figure 8*).

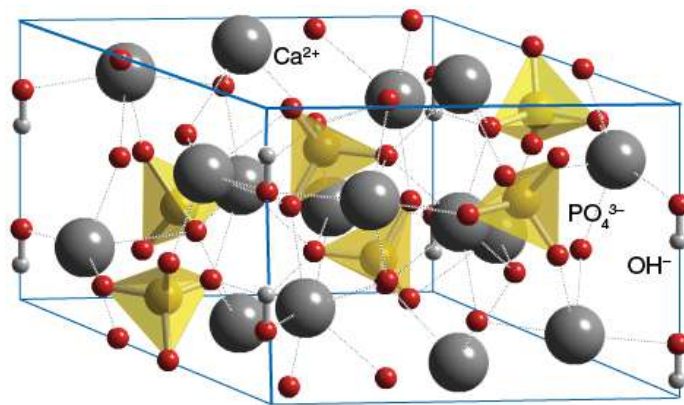


Figure 8: Hydroxyapatite crystal structure

However, given the complexity of its crystal lattice, hydroxyapatite can often contain variant ions, reticular defects and vacancies, which give origin to the class of non-stoichiometric or calcium-deficient hydroxyapatite.⁴⁸ For this reason, some forms of HAp can show a photocatalytic behavior in the presence of oxygen vacancies, which were generated by direct irradiation with UV light. It has been observed that depending on the type of oxygen atom that is missing in the crystalline structure, the light that this biomaterial is able to absorb changes due to the fact that its band gap is different. It seems that vacancies of oxygen atoms from the OH groups can result in a band gap of ~5 eV in the UVC region. However, this wavelength of light is not present in solar light at the Earth's surface due to the fact that it is being absorbed by the layer of atmospheric ozone. Therefore, pure hydroxyapatite usually does not display any photocatalytic activity under sunlight. In the presence of a vacancy of an entire OH group, there is the creation of a wide band gap between the allowed and forbidden bands responsible for the formation of optical spectral lines in the green-red visible region (521–743 nm). An oxygen vacancy in the phosphate (PO_4) groups significantly changes the forbidden energy

band gap, creating strong and fully-occupied energy levels inside the forbidden band, with excited and absorbed energy corresponding to UVA and violet/blue optical wavelengths. Lastly, the simultaneous oxygen vacancy in a phosphate group in combination with an OH vacancy leads to change the forbidden energy band gap, and also create a series of energy levels inside the forbidden band, which correspond to bands in the UVA-UVB regions and absorption peaks in the red-orange-yellow visible-light region.⁴⁹

The β -TCP ($\text{Ca}_3(\text{PO}_4)_2$) possesses a rhombohedral crystal system (*Figure 9*) and its structural arrangement allows a greater amount of Ca^{2+} and $(\text{PO}_4)^{3-}$ to be exchanged with the biological medium.⁵⁰ In the presence of an alkaline environment, TCP undergoes a slow transformation into the more insoluble HA form with the simultaneous absorption of water, which causes the complete destruction of the material's microstructure and a consequent increase of volume. In an acidic environment, there is the formation of dicalcium phosphate (DCP) and monocalcium phosphate (MCP).⁴⁷ From this, it follows that ceramic materials containing TCP in contact with water become unstable and are subject to a deterioration of their mechanical properties. However, the effect of water on monolithic ceramic objects made of TCP generally causes the formation of an insoluble layer of hydroxyapatite above the surface, which prevents its complete dissolution.

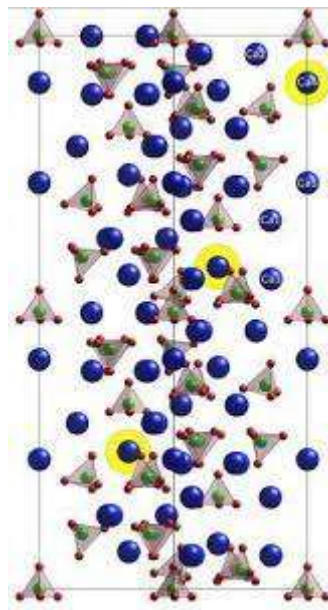


Figure 9: β -Tricalcium phosphate crystal structure

Normally, when both of the two forms of calcium phosphate coexist at different concentrations, there is the formation of the biphasic calcium phosphate (BCP) that is considered nowadays as the gold standard of bone substitutes in reconstructive surgeries.⁵¹ Despite the numerous advantages of CaP scaffolds, there are several circumstances where the use of a single material is not the best option to mimic the composition of natural bone. In this way, researchers started to develop composite materials that have demonstrated themselves to be more effective in enhancing both mechanical properties and bioactivity, compared to single ceramics and polymers.⁴¹ The goal of these synthetic scaffolds is not to permanently replace the bone tissue. Instead, they must stimulate bone growth and engage newly formed bone tissue, before being remodeled/resorbed. Therefore, regardless of the method of scaffold production, they should present a biomimetic surface, have an open porous microstructure for bone ingrowth, and should be biodegradable, having suitable degradation kinetics. In addition, the capacity to promote changes in the biological microenvironment to support cellular bone healing would be beneficial.

Materials and Methods

4. Synthesis procedures and analysis methods

4.1. Rapid sol-gel synthesis of Hydroxyapatite Nanoparticles

The synthesis of pure hydroxyapatite nanoparticles was achieved by performing two rapid sol-gel procedures that differ due to the use of calcium acetate hydrate, $\text{Ca}(\text{CH}_3\text{CO}_2)_2 \cdot \text{H}_2\text{O}$, or calcium nitrate tetrahydrate, $\text{Ca}(\text{NO}_3)_2 \cdot 4\text{H}_2\text{O}$, as starting precursors for calcium ions.⁵²

4.1.1. Hydroxyapatite powder from calcium nitrate tetrahydrate

Calcium nitrate tetrahydrate ($\text{Ca}(\text{NO}_3)_2 \cdot 4\text{H}_2\text{O}$, $\geq 99.0\%$, Fluka Analytical, Sigma-Aldrich) was dissolved in 100 mL of distilled water in a 250 mL beaker. Subsequently, orthophosphoric acid (H_3PO_4 , $\approx 85\%$, AnalaR, BDH Laboratory Supplies) at 85% w/w was added dropwise ($V_{\text{H}_3\text{PO}_4} = 4 \text{ mL}$) with a Pasteur pipet and the solution was heated at 45 °C at a fixed stirring rate of 500 rpm. Then the necessary amount of ammonium hydroxide (NH_4OH , sp. gr. about 0.89, AnalaR, BDH Laboratory Supplies) at 30% was added to reach a pH value between 7-8 that was kept constant during the synthesis. After 30 min, the synthesis was completed, and the final precipitate was immediately dried rapidly using a rotary evaporator (Buchi Rotavapor R-210 with glass assembly A) which operated for 1 h with a water bath temperature of 60 °C and under a constant pressure of 60 millibar, using a Buchi V-850 vacuum controller and Buchi V-700 diaphragm vacuum pump, and a 500 mL pear-shaped flask to hold the slurry. Afterwards, the precipitate was left overnight at room temperature in the rotary evaporator, under a constant pressure of 60 millibar, in order to obtain a white powder completely dried of pure hydroxyapatite nanoparticles.

This synthesis procedure was repeated three times (*Table 1*) in order to obtain the correct amount of HAp powder necessary to produce ceramic materials with different gradients of porosity.

Synthesis N°	Sample name	Mass of $\text{Ca}(\text{NO}_3)_2 \cdot 4\text{H}_2\text{O}$ (g)	Volume of NH_4OH (mL)
1	Nit(1)	23.51	16
2	Nit(2)	23.52	15.5
3	Nit(3)	23.52	13

Table 1: Mass of calcium nitrate tetrahydrate and ammonium hydroxide needed for the sol-gel synthesis of HAp from calcium nitrate tetrahydrate

4.1.2. Hydroxyapatite powder form calcium acetate monohydrate

Calcium acetate hydrate ($\text{Ca}(\text{CH}_3\text{CO}_2)_2 \cdot \text{H}_2\text{O}$, about 94%, Supelco, Sigma-Aldrich) was dissolved in 100 mL of distilled water in a 250 mL beaker. Subsequently, orthophosphoric acid (H_3PO_4 , $\approx 85\%$, AnalaR, BDH Laboratory Supplies) at 85% w/w was added dropwise ($V_{\text{H}_3\text{PO}_4} = 4 \text{ mL}$) with a Pasteur pipet and the solution was heated at 45 °C at a fixed stirring rate of 500 rpm. Then the necessary amount of ammonium hydroxide (NH_4OH , sp. gr. about 0.89, AnalaR, BDH Laboratory Supplies) was added to reach a pH value between 7-8 that was kept constant during the synthesis. After 30 min, the synthesis was completed, and the final precipitate was immediately dried rapidly using a rotary evaporator (Buchi Rotavapor R-210 with glass assembly A) which operated for 1 h with a water bath temperature of 60 °C and under a constant pressure of 60 millibar, using a Buchi V-850 vacuum controller and Buchi V-700 diaphragm vacuum pump, and a 500 mL pear-shaped flask to hold the slurry. Afterwards, the precipitate was left overnight at room temperature in the rotary evaporator, under a constant pressure of 60 millibar, in order to obtain a white powder completely dried of pure hydroxyapatite nanoparticles.

This synthesis procedure was repeated three times (*Table 2*) in order to obtain the correct amount of HAp powder necessary to produce ceramic materials with different gradients of porosity.

Synthesis N°	Sample name	Mass of $\text{Ca}(\text{CH}_3\text{CO}_2)_2 \cdot \text{H}_2\text{O}$ (g)	Volume of NH_4OH (mL)
1	Ac(1)	15.75	14.5
2	Ac(2)	15.74	12.5
3	Ac(3)	15.74	17

Table 2: Mass of calcium nitrate tetrahydrate and ammonium hydroxide needed for the sol-gel synthesis of HAp from calcium acetate hydrate

4.2. Preparation of the porous ceramic materials

Hydrogen peroxide (H_2O_2 , about 30%, GPR, BDH Laboratory Supplies) was added to the HAp powders to act as a pore forming agent. The newly synthesized hydroxyapatite powders ($m_{\text{theoric}} = 10 \text{ g}$) from both of the two sol-gel processes were reacted with a specific volume of hydrogen peroxide 30% w/w and diluted with the minimum amount of distilled water in order to obtain solutions having a different content of H_2O_2 and with the desired viscosity (Table 3). The viscous white solutions were slowly poured into ceramic molds to give them the shape of semi-spherical disks.

Sample name	Volume of H_2O_2 (mL)	Volume of H_2O (mL)
Nit(1)-5%	1.50	9.4
Nit(2)-3%	0.90	10.1
Nit(3)-3%	0.3	6.4
Nit(3)-5%	0.5	7.8
Nit(3)-10%	1.00	8.1
Ac(1)-5%	1.50	19.4

Ac(1)- >10%	~3	/
Ac(2)-3%	0.45	16.4
Ac(2)-10%	1.50	15
Ac(3)-3%	0.3	15.8
Ac(3)-5%	0.5	16.0
Ac(3)-10%	1.0	16.1

Table 3: Volumes of hydrogen peroxide and distilled water need for the preparation of the several porous ceramic materials

Regarding the sample labeled as Nit(2)-3%, half of the ceramic disks were heated for 8 h at 75 °C in order to promote the rapid evaporation of the water, while the other half of the ceramic samples were left to evaporate slowly at room temperature for 8 h to promote the gradual formation of bubbles due to the concentration of hydrogen peroxide.

Concerning the sample labeled as Ac(1)- >10%, it was synthesized by adding 1.5 mL of hydrogen peroxide to the remaining solution of the sample Ac(1)-5%. For this reason the correct amount of distilled water and the precise concentration of H₂O₂ are unknown.

In general, all the ceramic samples were placed in the desiccator, which contained lumps of blue silica gel, for some hours and then allowed to dry in the oven at 120 °C for a day. Subsequently the samples were removed from the ceramic molds and placed on alumina sheets in order to be sintered in the oven at different temperatures, with the programs shown in *Table 4*.

Settings	Program N°1	Program N°2
Ramp of temperature	100 °C/1 h to 700 °C	200 °C/1 h to 400 °C
Constant heating	700 °C for 2 h	400 °C for 2 h

Table 4: Settings of the programs used for the sintering of the several porous ceramic materials

4.3. Preparation of the porous scaffolds

Commercial hydroxyapatite powder (analytical HAp with $\geq 90\%$ purity) was also used to create a paste containing 40% v/v of HAp in order to produce different types of hand-made porous scaffolds (Table 5). In particular, 4 g of HAp powder was reacted with a specific volume of hydrogen peroxide 30% w/w and diluted with the necessary amount of distilled water to reach a total volume of 10 mL. Then, the minimum amount of sodium carboxymethylcellulose (CMC, degree of substitution 1.2, Sigma-Aldrich) was added in order to increase the viscosity of the paste.

Sample name	Volume of H ₂ O (mL)	Volume of H ₂ O ₂ (mL)	Mass of CMC (g)
HAp(CMC)-3%, 700 °C	9.6	0.4	1.9
HAp(CMC)-5%, 700 °C	9.4	0.6	2.4
HAp(CMS)-10%, 700 °C	8.8	1.2	2.9

Table 5: Mass of CMC and volumes of distilled water and hydrogen peroxide used for the preparation of different pastes containing 40 v/v of commercial hydroxyapatite powder

Afterwards, the same commercial HAp powder was also used to create a paste having a HAp/solvent ratio of 1:1 in order to avoid the employment of the sodium carboxymethylcellulose as additive. Specifically, 12 g of hydroxyapatite powder was mixed with a specific volume of hydrogen peroxide 30% w/w and diluted with the necessary amount of distilled water to reach a total volume of 12 mL (Table 6).

Sample name	Volume of H ₂ O (mL)	Volume of H ₂ O ₂ (mL)
HAp-700 °C	12	/

Sc-3%, 700 °C	10.9	1.1
Sc-5%, 700 °C	10.2	1.8
Sc-10%, 700 °C	8.4	3.6

Table 5: Volumes of distilled water and hydrogen peroxide used for the preparation of different pastes containing commercial hydroxyapatite powder

Then, the several pastes were loaded into a commercial plastic syringe (capacity of 5 mL and tip diameter of 2 mm) and manually extruded allowing the creation of the scaffolds having different dimensions and number of layers. Afterwards, all the samples were placed on alumina sheets (50 mm x 100 mm x 0.889 mm, Hybrid Laser Tech) and sintered in the oven by setting the program with a ramp of temperature of 100 °C/1 h to 7 h and a period of constant heating at 700 °C for 2 h.

4.4. Characterization analysis

4.4.1. X-Ray diffraction

The mineralogical composition of the powders was assessed by X-ray powder diffraction (XRD). XRD was conducted on a θ/θ diffractometer (Malvern, PANalytical, X'Pert Pro3, The Netherlands), equipped with a fast RTMS detector (Malvern PANalytical, PIXcel 1D, The Netherlands), using Cu K α radiation (45 kV and 40 mA, 10-80° 2 θ range, with a virtual step scan of 0.020° and virtual time per step of 2 s at room temperature). For this analysis, the samples were ground, in an agate mortar, until the whole sample passed through a 63 μ m sieve. The phase identification was executed using the PANalytical X'Pert High Score Plus PRO3 software.

4.4.2. Scanning electron microscopy and Optical microscopy

The morphology of the powders and the microstructure of the prepared monoliths were first evaluated in an optical microscope (Leica EZ4HD, Germany)

and then observed by scanning electron microscopy (SEM, Hitachi, SU-70, Tokyo, Japan) with an accelerating voltage of 15 kV. Before SEM examination, the samples were placed with conducting carbon cement (Leit-C, Conducting Carbon Cement, AGG3300, Germany) on adequate supports for SEM visualization, then dried in the oven at 60 °C and coated with a carbon thin film (Emitech, K950, USA) to provide a conducting layer.

4.4.3. Specific surface area with BET method

The specific surface area (SSA) of the ceramic samples and the scaffolds synthesized with 10% of hydrogen peroxide was measured by physical nitrogen adsorption isotherms (outgas temperature: 150 °C) using the Brunauer-Emmett-Teller (BET) method (Micromeritics, Gemini 2370 V5.00, Norcross, GA, USA).

4.5. Biomineralization assay with simulated body fluid

4.5.1. Simulated body fluid solution preparation

In order to produce 1 L of simulated body fluid (SBF),⁵³ 700 mL of deionized (DI) water was placed in a 1 L polypropylene beaker and set at 37 ± 1.0 °C in a water bath. The solution was continuously stirred throughout. The reagents were slowly added to the DI water in the order given in *Table 7* with an accuracy of ± 0.1 mg. The pH was monitored (Thermo Scientific Orion Star A211 pH meter calibrated with three standards of pH 4.01, 7.00 and 10.04, respectively) and kept at pH 7.4 in order to avoid any rapid increase, which would cause precipitation. Once the reagents were mixed, the SBF solution was transferred to a 1 L volumetric flask and filled to the mark with deionized water, and cooled down to room temperature. Then the SBF was stored in the refrigerator at 5 °C.

Order	Reagent	Amount (g)	CAS number
-------	---------	------------	------------

1	NaCl	8.036	7647-14-5
2	NaHCO ₃	0.352	144-55-8
3	KCl	0.225	7447-40-7
4	K ₂ HPO ₄ · 3H ₂ O	0.230	16788-57-1
5	MgCl · 6H ₂ O	0.311	7791-18-6
6	HCl	40 mL	7647-01-0
7	CaCl ₂ · 6H ₂ O	0.293	7774-34-7
8	Na ₂ SO ₄	0.072	7757-82-6
9	Tris	6.063	77-86-1

Table 7: Mass of the reagents used for the preparation of SBF and order in which they needed to be added to the deionized water

4.5.2. Bioactivity of the scaffolds based on concentration

The bioactivity of the scaffolds was tested by immersing the materials in SBF using a 22 mg piece of scaffold added to 14.5 mL SBF in an airtight polyethylene container, previously sterilized for 10 min under a UV lamp (STERIL BOX germicidal UV lamp). Dissolution vessels were placed in an oven held at 37 °C and incubated for three different time points: 1 day (a), 3 days (b) and 7 days (c). At the end of each period, the samples were removed from the incubator and the solids were collected by filtration (particle retention 1-2µm). The pieces of scaffold were immediately washed three times with DI water and the filtered SBF solution was collected to measure the final pH and determine the temperature. Each washed sample was left to dry in the oven at 37 °C overnight, and then prepared for the SEM analysis.

4.5.3. SEM visualization of the immersed scaffolds

The ceramic samples and the scaffolds, which were immersed in SBF for 1 day, 3 days and 7 days, were collected and analyzed by scanning electron microscopy (SEM, Hitachi, SU-70, Tokyo, Japan) with an accelerating voltage of 15 kV. To prepare them for analysis, first they were washed several times in order to stop deterioration and dried in the oven at 37 °C for one day. Afterwards the samples were placed with conducting carbon cement (Leit-C, Conducting Carbon Cement, AGG3300, Germany) on adequate supports for SEM visualization, then dried in the oven at 60 °C and coated with a carbon thin film (Emitech, K950, USA) to provide a conducting layer.

4.6. Mechanical tests

4.6.1. Measurement of the dimension of the scaffolds

The dimensions of the three scaffolds were measured by using a stainless steel vernier digital caliper with a liquid-crystal display, having an accuracy of ± 0.01 mm. The values reported in *Table 8* are related to the dimensions of the cuboidal scaffolds composed of 4 layers, each of which made up of 4 filaments, and alternated with 3 layers made up of 5 filaments each, for a total of 7 layers.

Sample name	Width (mm)	Thickness (mm)	Height (mm)
Sc-3%	19.51	16.68	13.26
Sc-10%	21.62	18.55	14.76

Table 8: Dimensions of the scaffolds considered for the mechanical tests

4.6.2. Testing machine

Then the compressive strength was determined by performing uniaxial tests on scaffolds synthesized with 3% and 10% of hydrogen peroxide. Tests were carried out in air using a universal testing machine (AG-IS 200N, Shimadzu Corporation, Kyoto, Japan) with a 200 N load cell in the perpendicular direction of the printing

plane at a constant speed of 0.5 mm/min. The compressive strength (σ) of the structures was calculated by using the following formula:

$$\sigma = \frac{F_{\text{applied}}}{A}$$

where F_{applied} is related to the maximum applied load and A stands for the measured square area section of the sample.

4.7. Photocatalytic tests

The photocatalytic activity of the scaffolds was evaluated in liquid–solid phase, monitoring the degradation of an organic dye, methylene blue (MB, $\geq 82.0\%$, Sigma-Aldrich), using a spectrometer (Shimadzu UV 3100, JP). The tests were performed at room temperature, in a cylindrical beaker containing an aqueous solution of the dye (500 mL), at an initial concentration of 5 mg/L. Before the photocatalytic degradation experiment was conducted, the samples were ground in an agate mortar, until the whole sample passed through a 75 μm sieve, and the powders obtained were added to the initial dye solution in order to have a concentration of the photocatalyst in the slurry equal to 0.25 g/L. In order to mix the solution thoroughly, the slurry was magnetically stirred throughout the reaction; the reactor was covered with a watch-glass, so as to avoid the evaporation of the solution. Concerning the lighting of the reacting system, two lamps were positioned at either side of the reactor at a distance of 5 cm. The UV/visible-light source employed was two fluorescent lamps (Philips master PL-S 2P 9W/840, NL), having an irradiance of 50 Wm^{-2} in the visible region and 0.6 Wm^{-2} in the UVA region to mimic natural sunlight. During the experiments, the photocatalytic degradation of MB was monitored by sampling about 4 mL of the slurry from the reactor, at regular time intervals (1 h, 2 h, 4 h, 6 h, 8 h and 12 h). Before switching the lamps on, the suspension was stirred in the dark for 30 min, with the aim of allowing the adsorption of MB onto the powders. The powders in the samples were left in the dark overnight to allow the deposition of the particles on the bottom of the tube, allowing an easy removal of the dye solution. Then the MB concentration in the liquid was determined, taking advantage of the Lambert–Beer law, by measuring the absorbance in a spectrometer at a

wavelength of 665 nm, using distilled water as a reference. The extent of MB photocatalytic degradation (ω) was evaluated as follows:

$$\omega (\%) = \frac{C_0 - C_s}{C_0} \cdot 100$$

where C_0 is the initial MB concentration and C_s is the concentration after a certain UVA/visible irradiation time (the total irradiation time was set at 12 h). Control experiments (adsorption of the MB dye) in the dark were performed prior to testing the photocatalytic activity of the prepared samples. In particular by taking 4 mL of the slurry from the reactor at different time intervals: 30 minutes, 1 h, 2 h, 4 h and 6 h.

4.8. In vitro study: biocompatibility test

4.8.1. MTT assay

The cytocompatibility of the hydroxyapatite (HAp) materials was determined using the thiazolyl blue tetrazolium bromide (MTT) assay. Cells were seeded in two different 96-well plates in the presence of HAp samples, at a density of 5.0×10^3 and 1.0×10^4 per well, and incubated at 37 °C in 5% CO₂ for 24 hours. The medium was then removed and replaced within a serum-free medium containing 2 mg/mL MTT and incubated for 2 h at 37 °C. The MTT reagent was then removed, and the formazan crystals were solubilized using dimethyl sulfoxide (DMSO). The absorbance of the solution at 570 nm was measured on a microplate reader (CLARIOstar Plus, BMG Labtech). The absorbance of the controls was subtracted, and the percentage control was calculated as the absorbance of the treated cells/control cells. Cell viability was assessed using the equation:

$$\text{Cell viability (\%)} = \frac{\text{Absorbance of the tested samples}}{\text{Absorbance of the control sample}} \cdot 100$$

Results and Discussions

5. Characterization of the samples

Due to the large number of samples, it was decided to compare the XRD plots and SEM images only of the ceramic samples derived from the third sol-gel synthesis (Nit(3) and Ac(3)) and the scaffolds produced using commercial hydroxyapatite and hydrogen peroxide, without the addition of sodium carboxymethylcellulose (Sc-3%, Sc-5% and 10%).

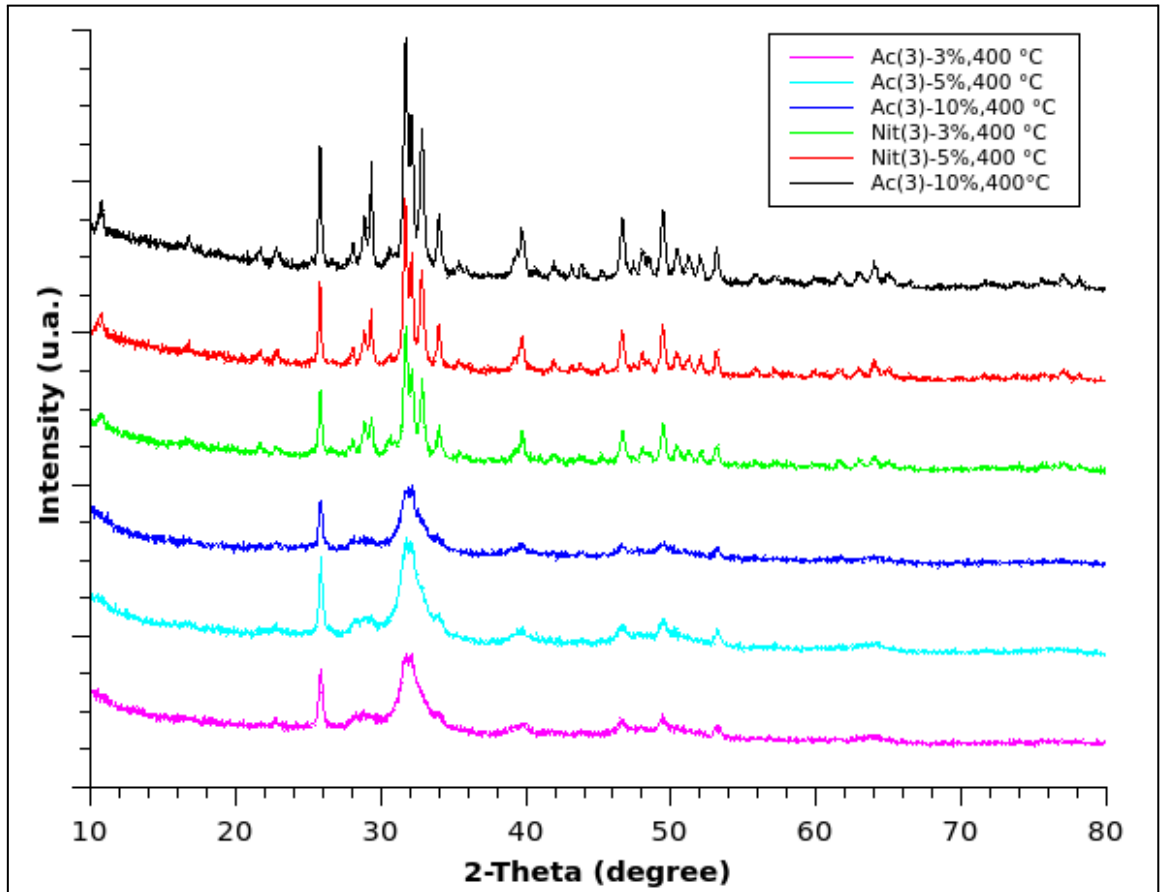
Regarding the specific surface area, it was decided to carry out the analysis only on the samples containing 10% hydrogen peroxide.

5.1. X-Ray Diffraction

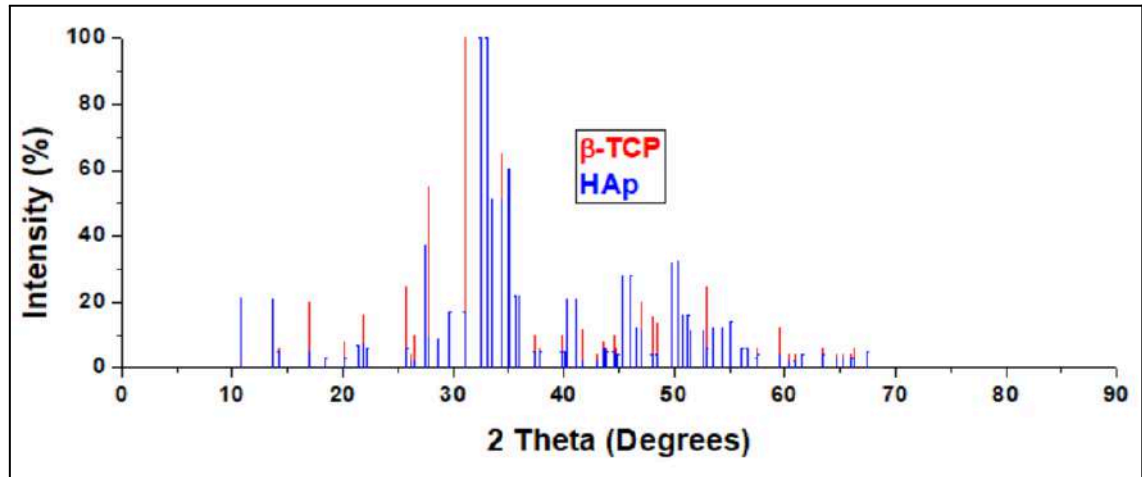
X-ray powder diffraction (XRD) is a rapid non-destructive analytical technique primarily used for phase identification of a crystalline material, and can also provide information on unit cell dimensions and the spacing and planes of atoms. Diffraction occurs when the light is scattered elastically by the electrons (scatterers), belonging to a periodic array of atoms with long-range order, and consequently there is the formation of spherical waves that can produce constructive interference at specific angles, determined by Bragg's law ($n\lambda=2d\sin\theta$). For this reason, amorphous materials, like glass, do not produce a diffraction pattern. The scattering of X-rays from the atoms produces a diffraction pattern, which contains information about the atomic arrangement within the crystal, and it is a product of the unique crystal structure of a material. The peak profiles contain information about crystallite size, strain and nanostructure. For this reason, this technique is commonly applied to characterize minerals, ceramics, metals and alloys, catalysts, polymers, pharmaceuticals, organic compounds, environmental and forensic samples, among others.

Taking into account the XRD patterns of all the samples sintered at 400 °C (*Graph 1*), it is possible to clearly see the differences between the profiles of the samples synthesized from calcium acetate, which appear to be more broad and lower in intensities, compared to the ones synthesized with calcium nitrates, which seems to possess a sharp appearance. The broadening and the low intensity of the peaks of calcium acetate

depend on the low sintering temperature. During this process, the acetate that was used as starting precursor for calcium ions does not completely decompose, which leaves some carbon atoms inside the HAp lattice. Despite the low temperature of sintering, all the nitrate and acetate ceramic samples are made of pure HAp, since the patterns do not have peaks that can be related to the reference pattern of the TCP (*Graph 2*).

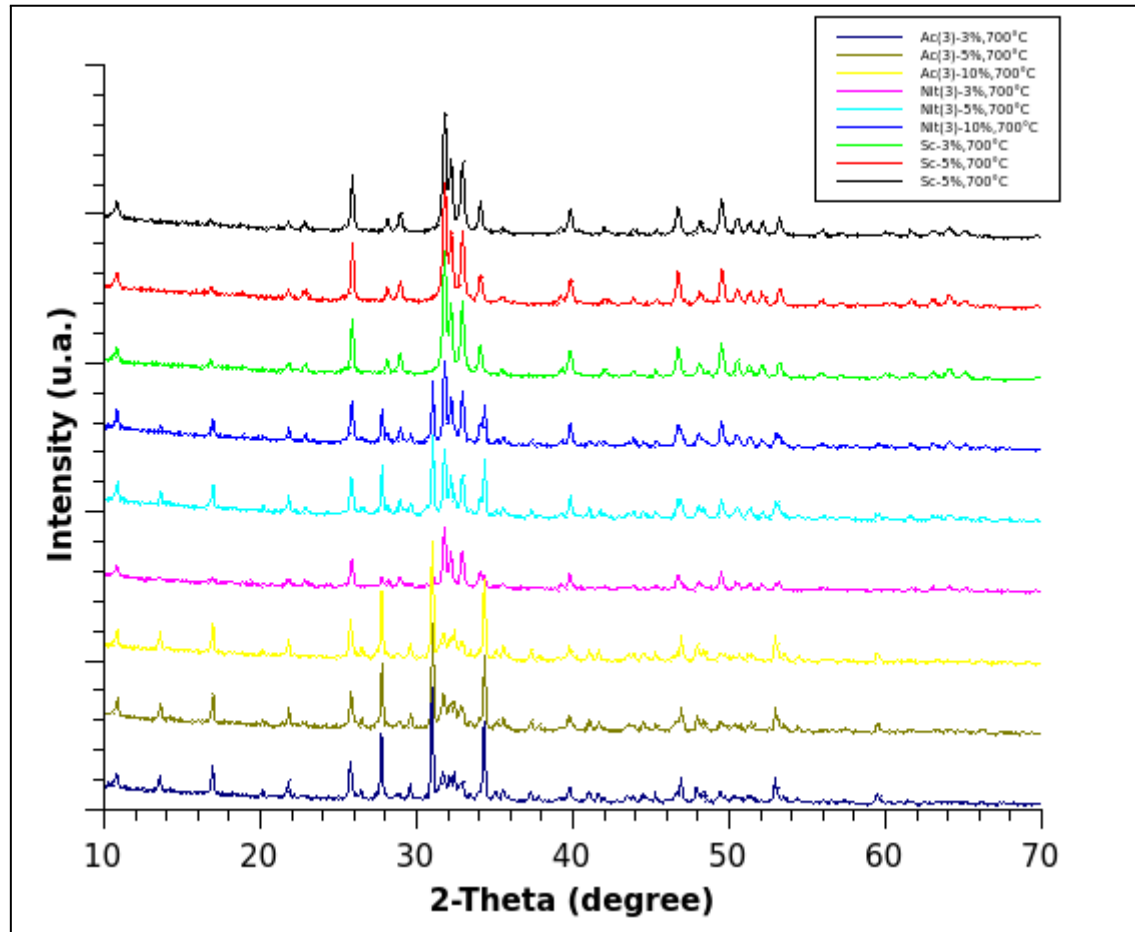


Graph 1: XRD patterns of the ceramic samples synthesized with calcium nitrate and calcium acetate, all sintered at 400 °C, in comparison to the XRD reference patterns of HAp and TCP



Graph 2: XRD reference patterns of HAp and TCP

The XRD patterns of the samples sintered at higher temperature (*Graph 3*) show the presence of sharp peaks that have high intensity and fall at the same angle values. However, by looking at the reference XRD pattern of HAp and TCP, it seems that all the samples contain hydroxyapatite. However, the presence of the peak with a high intensity that falls around a 2-theta value of 31 degree can suggest that maybe there is a small quantity of TCP inside of each sample (*Graph 2*). The calcination temperature of 700 °C is high enough to form the hydroxyapatite phase, but is not sufficient to form the β -TCP phase, since usually it requires a higher temperature. Therefore, this incorrect peak assignment could be due to the fact that the reference pattern for hydroxyapatite may not be the best one to use. At first, in the database it had been found three different reference patterns for the hydroxyapatite. Therefore, it might have been appropriate to use a different one, although the current one perfectly corresponds to the experimental data of the samples sintered at lower temperature.



Graph 3: XRD patterns of the ceramic samples synthesized with calcium nitrate, calcium acetate, and the scaffold synthesized with commercial HAp powder, all sintered at 700 °C in comparison with the XRD reference patterns of HAp and TCP

5.2. Scanning electron microscopy and Optical microscopy

The morphology and structure of the ceramic materials and scaffolds of hydroxyapatite have been thoroughly evaluated through the application of microscopy techniques in order to observe the samples at different scales. Optical microscopes, also called light microscopes, are a type of microscope that uses a beam of visible light (ranging from 400 nm to 650 nm) and a system of lenses to generate magnified images (typically < 1500x) of a specimen. However, its resolution (the resolving power) is theoretically limited to approximately one-half the wavelength of visible light (200 nm), which limits the types of materials and structures that it is possible to observe. In contrast, a scanning electron microscope (SEM) is a type of electron microscope that produces images of

microstructure and morphology of a sample by scanning it with a focused beam of electrons. It has higher magnification (typically >100,000x) and resolution, but also greater depth of field due to the geometry of the imaging system, which allows the visualization of the whole specimen to be in focus. SEM can create a three-dimensional appearance of the specimen image due to the fact that one of its detectors collects information from the secondary electrons (SEs), which originate from superficial atoms composing the sample surface (topography).

Considering the images obtained from the optical microscope, it is possible to notice that the surface of all the samples is very irregular with the presence of pores and cavities of different sizes. It is noticeable that the samples coming from different synthetic processes or sintered at different temperatures can be recognizable by their color. In fact, the samples synthesized with calcium nitrate are all white, while the three scaffolds of commercial hydroxyapatite have a distinguishable light blue color. This is an indicator of possible photocatalytic behavior of the HAp, since the color originated from oxygen vacancies.⁴⁹ Regarding the ceramic samples produced with calcium acetate, the three that were sintered at the temperature of 400 °C assumed a brownish color, while the other three sintered at 700 °C possessed a bright white color. This difference is due to the presence of a small quantity of residual carbon (from the acetate) that did not react due to the lower temperature and remained inside the samples.


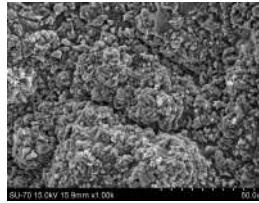
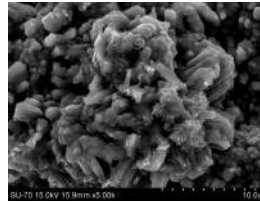

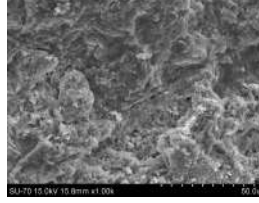
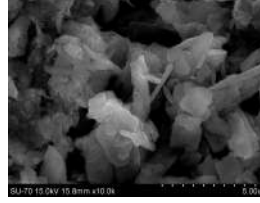
Taking into account the SEM images at different magnifications (x 1.00 k, 5.00 k, 10.0 k) and a distance from the sample (WD) maintained at around 14-20 mm, it is possible to clearly see the general topography of the samples' surface and the fine microstructure of the hydroxyapatite crystals (*Table 9*).


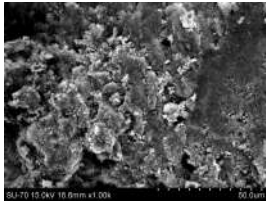
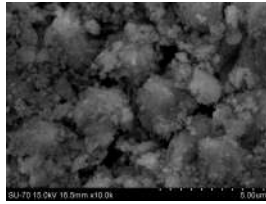
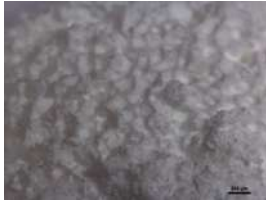
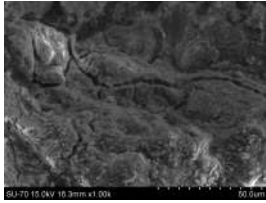
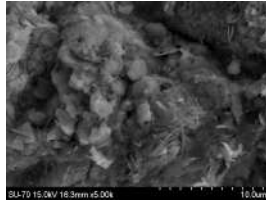

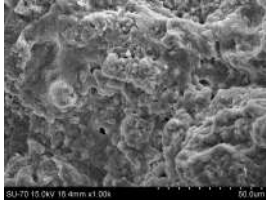
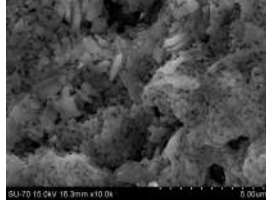

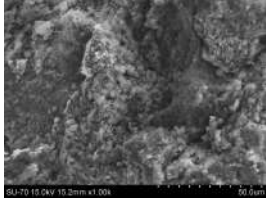
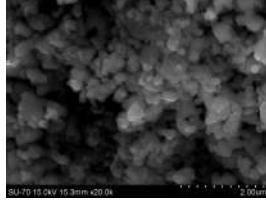

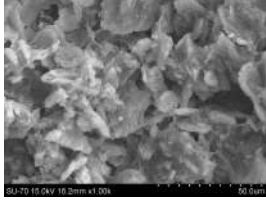
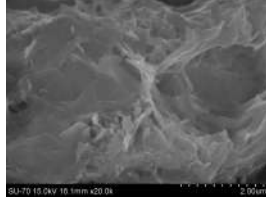

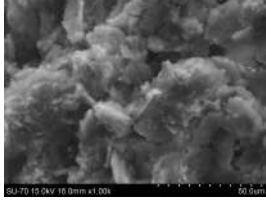

The six samples obtained from the sol-gel synthesis of calcium nitrate display a rough surface composed of many compacted and compressed layers. The presence of plate-like and needle-like crystalline structures is directly dependent on the percentage of hydrogen peroxide added and on the sintering temperature. In fact, by observing the sintered samples at a lower temperature, it is possible to notice that hydroxyapatite has formed more plate-like crystal structures at lower hydrogen peroxide concentrations. For this reason, with the increase of H₂O₂ content, hydroxyapatite particles tend to assume a more grain-like structure. In calcium nitrate samples sintered at higher temperatures, the

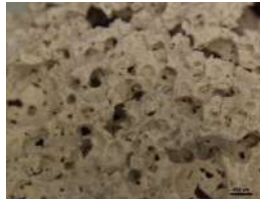
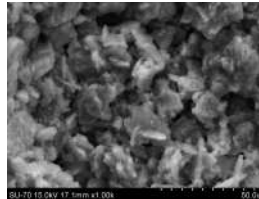
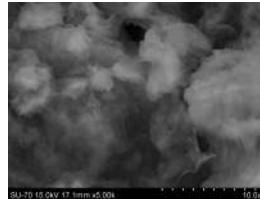

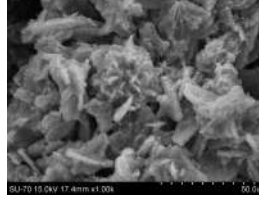
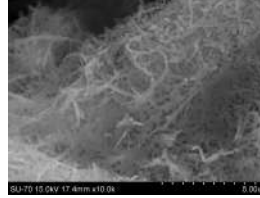

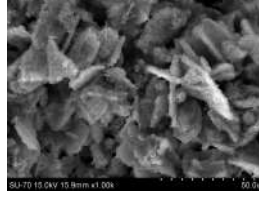
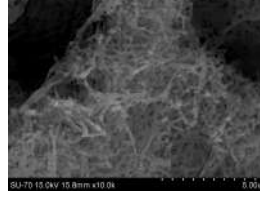

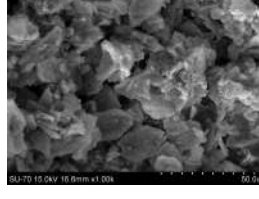
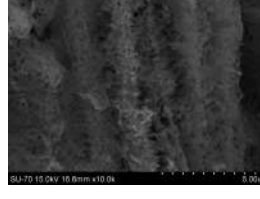

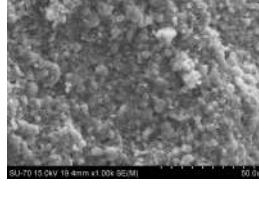
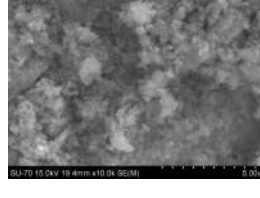

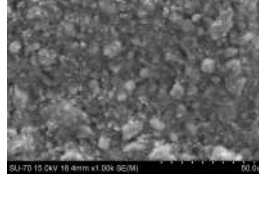
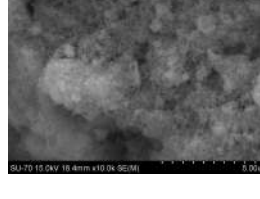
presence of these grains, due to the agglomeration of larger HAp particles, is more marked. As a matter of fact, it is possible to observe the presence of larger and more compact crystals already at lower percentages of peroxide.

Regarding the samples synthesized from calcium acetate, they display a surface composed of many plate-like crystal structures oriented in different directions, but that seems to grow perpendicular with respect to the surface. The alignment and the formation of these large, well-defined crystalline structures were better achieved in the acetate samples sintered at a higher temperature. This fact is confirmed by the needle-like microstructures that are clearly visible in the SEM images taken at higher magnification.

Meanwhile, the three scaffolds made of commercial hydroxyapatite seem to possess a compact superficial surface constituted of aggregates of plate-like structures, horizontally aligned, that fuse together in order to form layers that superimpose one another. By looking at these plate structures with a higher magnification, it is possible to notice that they are formed by an assembly of HAp particles as grains. In particular, knowing that the samples were sintered at the same temperature, it is possible to observe that the dimensions of these grains seem to increase with the increase of the percentage of hydrogen peroxide.

Sample name	Optical microscopy	Scanning Electron Microscopy (SEM)	
Nit(3)-3%, 400 °C			
Nit(3)-5%, 400 °C			

<p>Nit(3)-10%, 400 °C</p>			
<p>Nit(3)-3%, 700 °C</p>			
<p>Nit(3)-5%, 700 °C</p>			
<p>Nit(3)-10%, 700 °C</p>			
<p>Ac(3)-3%, 400 °C</p>			
<p>Ac(3)-5%, 400 °C</p>			

Ac(3)-10%, 400 °C			
Ac(3)-3%, 700 °C			
Ac(3)-5%, 700 °C			
Ac(3)-10%, 700 °C			
Sc-3%, 700 °C			
Sc-5%, 700 °C			

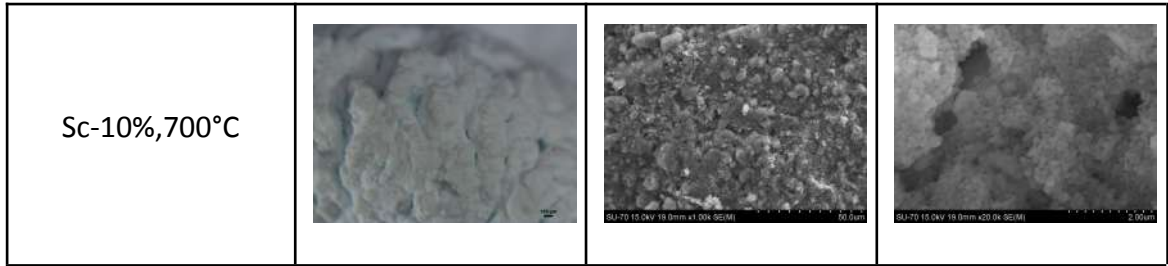


Table 9: Optical microscope and SEM images of the several ceramic materials and scaffolds synthesized from calcium nitrate tetrahydrate (Nit), calcium acetate hydrate (Ac) and commercial HAp (Sc)

5.3. Specific surface area

The phenomenon of adsorption is the adhesion of atoms, ions or molecules from a gas, liquid or dissolved solid to a surface. This process creates a film of the *adsorbate* (molecules or atoms accumulated) on the surface of the *adsorbent*. For this reason, the adsorption is considered a surface phenomenon and it is strictly related to the surface energy. In a bulk material, all the internal atoms are bonded together in order to completely fulfill the bonding requirements. However, atoms on the surface of the adsorbent are not wholly surrounded by other adsorbent atoms and, therefore, can easily attract atoms or molecules of adsorbate. The exact nature of the bonding depends on the details of the species involved, but the adsorption process is generally classified as physisorption, characteristic of weak van der Waals forces, or chemisorption, in which there is the formation of covalent bonds.

The adsorption of gasses and solutes is usually described through isotherms, that are obtained by relating the amount of adsorbate on the adsorbent as a function of its pressure (gas) or concentration (for liquid phase solutes) at constant temperature. Various different isotherm models have been developed in the last decades, but the one used for the analysis of the surface area of the various samples is the Brunauer-Emmett-Teller model. The BET theory relies on the assumptions that the gas molecules physically adsorb on the solid in layers infinitely, and there is no interaction between each adsorption layer, which allows one to apply the Langmuir theory singularly. By comparing the different adsorption isotherm classified by IUPAC (*Figure 10*) and those obtained from the porous ceramic samples, synthesized from calcium nitrate tetrahydrate and calcium acetate, and the scaffolds having 10% hydrogen peroxide (*Figure 11*), it is

possible to obtain much useful information about the surface and the type of porosity present, which are classified as micropores (< 2 nm), mesopores (2-50 nm) and macropores (> 50 nm, the limit of this technique being up to about 200 nm).

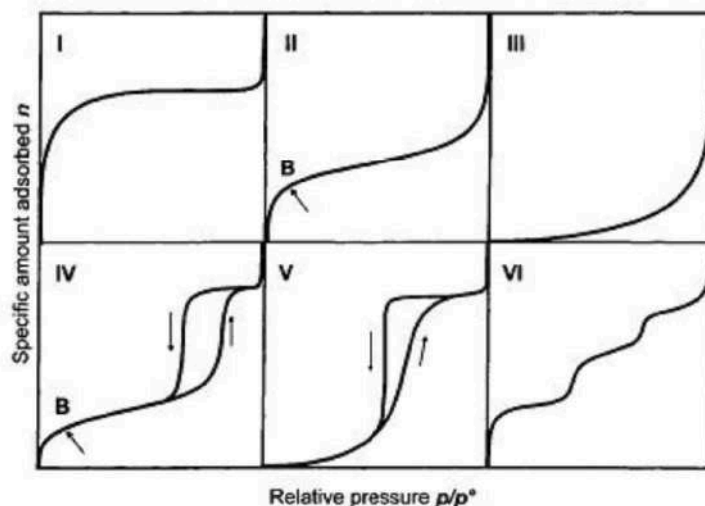


Figure 10: IUPAC classification of the different types of adsorption isotherm

A Type I isotherm is given by microporous solids with relatively small external surfaces that are able to adsorb the gas molecule forming a monolayer.

A Type II isotherm is associated with an adsorption that occurs on a macroporous or non-porous solid. They indicate the formation of a layer of adsorbate whose thickness progressively increases with the relative pressure values tending to 1 (unrestricted monolayer-multilayer adsorption). The knee present to this type of isotherm (point B in *Figure 10*) indicates the pressure at which it forms the adsorbed monolayer and the beginning of the formation of the molecular multilayer.

A Type III isotherm has a convex shape and it also indicates unrestricted multilayer formation process. It forms because lateral interactions between adsorbed molecules are strong in comparison to the weak interactions between the adsorbate and the adsorbent surface.

A Type IV isotherm is characterized by an initial trend similar to that of Type II (monolayer-multilayer adsorption) but differently it tends to stabilize at high relative pressure values. This curve is obtained when the adsorption on mesoporous solids proceeds via multilayer adsorption directly followed by capillary condensation in pores,

which results in the formation of the hysteresis loop that is obtained from the desorption process of the gas which does not follow the the same path as adsorption.

A Type V isotherm, like Type III, is indicative of weak adsorbate-adsorbent interactions. It also exhibits a hysteresis loop, which indicates that there is the formation of multilayers on the surface of the mesoporous solid followed by the process of capillary condensation.

A Type IV isotherm represents stepwise multiplayer adsorption on a uniform and non-porous solid surface. The steps, whose sharpness depends on the system and the temperature, indicate the filling stages of individual layers.

Therefore, by looking at the isotherms of the samples (*Figure 11*), it is possible to assume that they can be classified as Type V isotherms, in which there is only multilayer adsorption, and hysteresis from capillary condensation in mesopores. This is achieved due to the fact that lateral interactions between the adsorbed N₂ molecules are strong in comparison to the interactions between the adsorbent surface and the adsorbate (N₂).

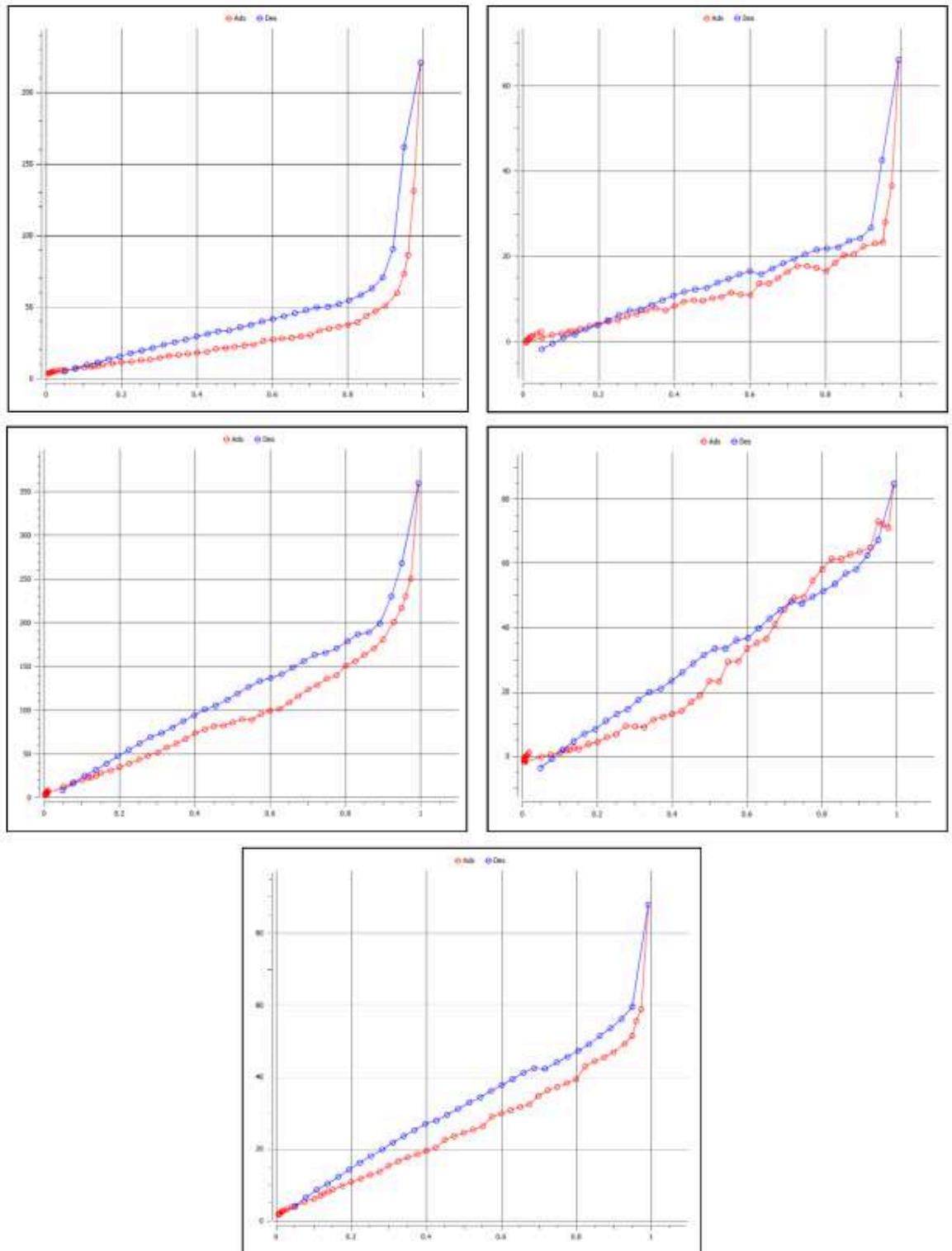


Figure 11: Adsorption isotherms of the four porous ceramic samples, synthesized from calcium nitrate tetrahydrate (top), calcium acetate (middle), and the commercial HAp scaffold (bottom), all having 10% hydrogen peroxide

Considering the IUPAC classification of the hysteresis forms (*Figure 12*), the hysteresis loops associated with capillary condensation taking place in the mesopore samples can be considered as something between H3 and H4. In particular, H3 is often traced back to the presence of interstitial slit-like pores due to aggregates of platelike particles. Meanwhile, H4 is attributed to the presence of narrow slit-like pores and the capillary condensation of particles with internal voids of irregular shape and broad size distribution.

Consequently, the samples have a broad size distribution of platelike (or needle) particles, forming slit-like pores, that possess smaller internal voids of irregular shape. Probably the slit-like pores are mesopores and the internal pores could be mesopores or micropores.

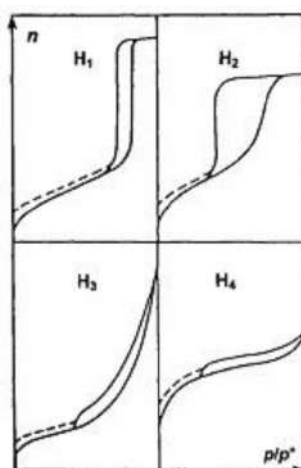


Figure 12: IUPAC classification of the four different shapes of hysteresis loops

Considering the specific surface area of the samples (*Table 10*) obtained from the BET method, it is possible to notice that the scaffold of commercial HAp, both of the ceramic samples synthesized with calcium nitrate tetrahydrate and the one synthesized with calcium acetate sintered at 700 °C have similar SSA values in the range of 46-62.7 m²/g. Meanwhile, the sample synthesized with calcium acetate and sintered at 400 °C has a SSA of 232.3 m²/g, which is four/five times greater with respect to the other values. This could be explained by the fact that the sample still contains some carbon that is well known to produce high SSA materials.

Sample name	SSA from BET (m ² /g)	SSA from BJH (m ² /g)	Pore radius from BJH (nm)
Nit(3)-10%, 400 °C	49.8	60.9	1.66
Nit(3)-10%, 700 °C	46.0	29.4	2.13
Ac(3)-10%, 400 °C	232.3	202.5	1.57
Ac(3)-10%, 700 °C	21.8	81.4	1.94
Sc-10%, 700 °C	62.7	50.3	1.66

Table 10: Comparative table with surface area from BET and BJH, and the pore size from BJH of the ceramic material and scaffold synthesized from calcium nitrate tetrahydrate, calcium acetate hydrate and commercial HAp, all having 10% hydrogen peroxide

Regarding the pore size, the SSA and radius of the pores present in the samples were determined by using the BJH (Barrett, Joyner and Halenda) analysis, which provides approximate pore volumes of pores with diameters between 2 nm (mesopores) and 300 nm (macropores). This method cannot accurately detect micropores, and for this reason the SSA obtained from this analysis is less precise compared to the SSA from BET. However, it is possible to roughly estimate the SSA due to microporosity by taking the difference between the values of SSA from the BET and the BJH analysis (*Table 11*). In particular, three of the five samples have SSA values due to their microporosity within the range of 12.4-29.8 m²/g. Therefore, the percentage of the specific surface area due to their microporosity is estimated to be around 11-15% of the total specific surface area determined by the BET method. This means that most of the SSA comes from the presence of many mesopores, having a diameter between 3-5 nm.

Sample name	SSA from BET (m ² /g)	SSA from BJH (m ² /g)	Estimated SSA due to microporosity
-------------	-------------------------------------	-------------------------------------	---------------------------------------

			(m ² /g)
Nit(3)-10%, 400 °C	49.8	60.9	/
Nit(3)-10%, 700 °C	46.0	29.4	16.6
Ac(3)-10%, 400 °C	232.3	202.5	29.8
Ac(3)-10%, 700 °C	21.8	81.4	/
Sc-10%, 700 °C	62.7	50.3	12.4

Table 11: Comparative table with surface area from BET method, BJH analysis and the SSA due to the microporosity pore size from BJH of the ceramic material and scaffold synthesized from calcium nitrate tetrahydrate, calcium acetate hydrate and commercial HAp, all having 10% hydrogen peroxide

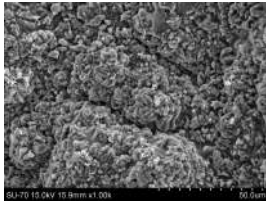
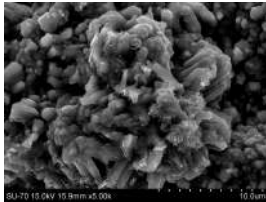
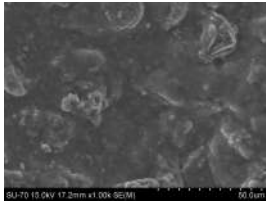
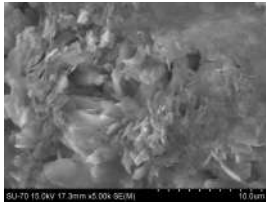
5.4. Bioactivity test: SEM visualization after SBF

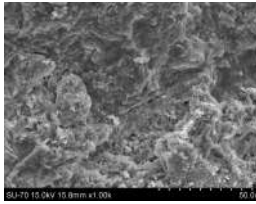
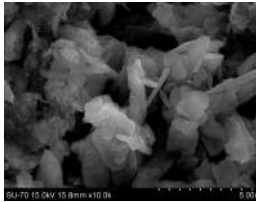
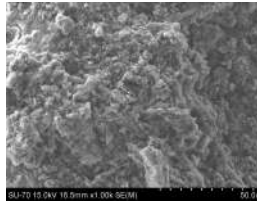
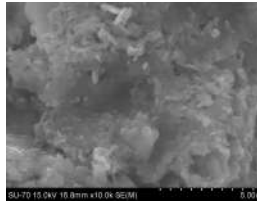
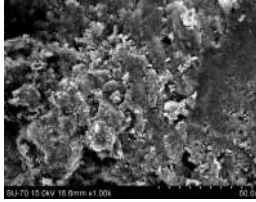
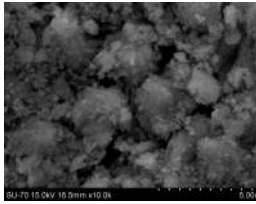
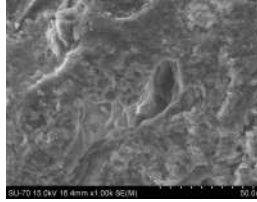
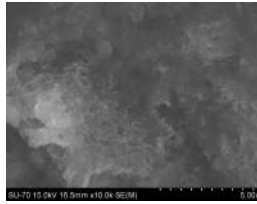
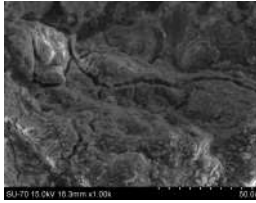
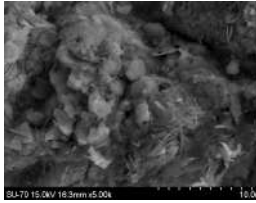
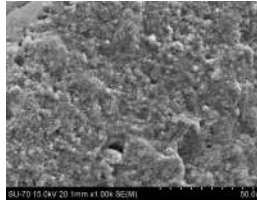
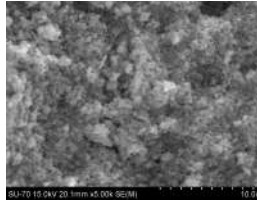
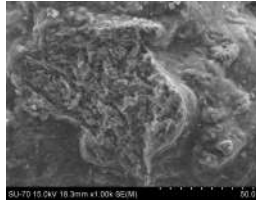
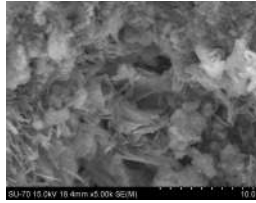
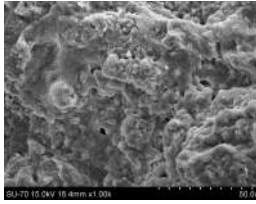
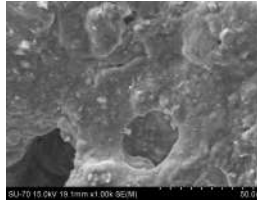
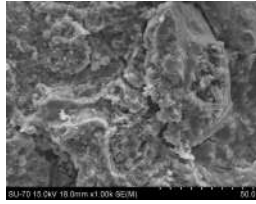
The morphology and structure of the ceramics material and scaffolds of hydroxyapatite, before and after their immersion in SBF, have been thoroughly evaluated through the application of the scanning electron microscopy technique. The SEM images taken at different magnifications (x 1.00 k, 5.00 k, 10.0 k) allowed me to visualize the new coating layer of hydroxyapatite that grew on the sample surface. From *Table 12*, it is noticeable the absence of the images of all the samples retrieved after 7 days of immersion into SBF and this is due to the fact that we first tried to perform an XRD analysis (at very low angle) on the coated surface. The specimens were attached to the XRD sample holders through the use of a fixative paste. The problem was that most of the HA samples shattered while trying to retrieve them in order to perform the SEM.

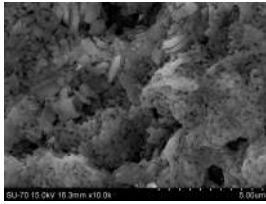
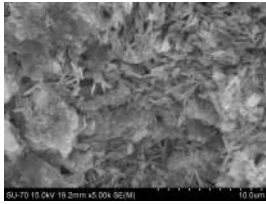
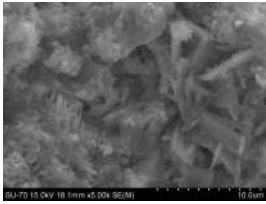
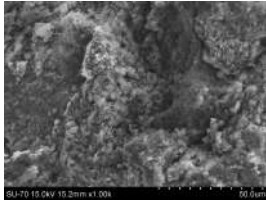
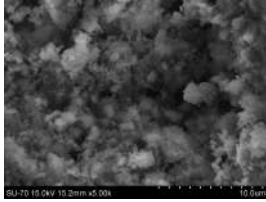
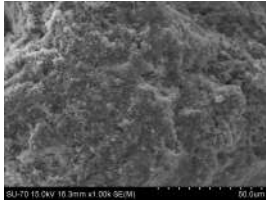
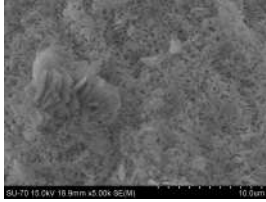
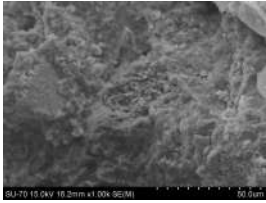
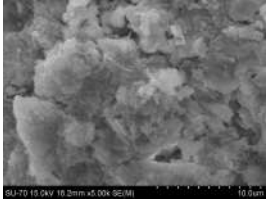
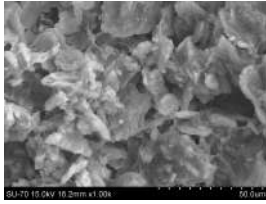
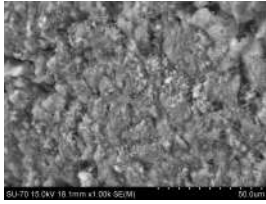
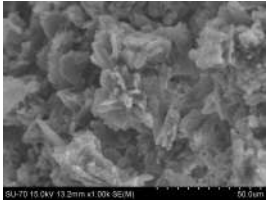
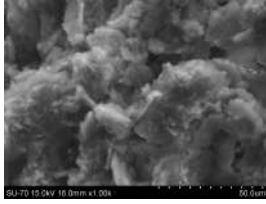
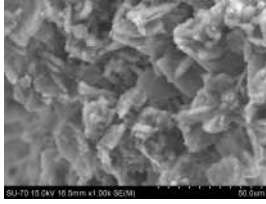
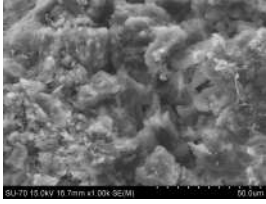
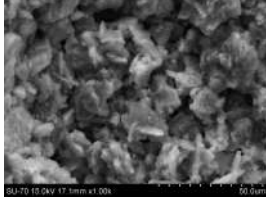
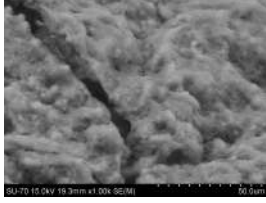
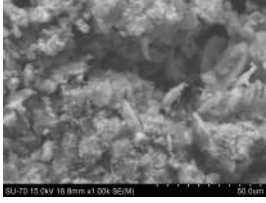
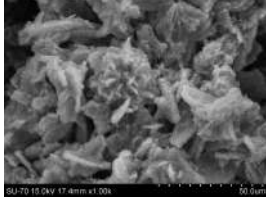
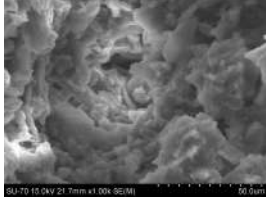
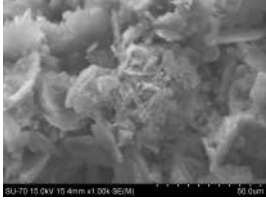
Regarding the samples obtained from the sol-gel synthesis of calcium nitrate and sintered at 400 °C, it is clearly visible that there was the formation of the new hydroxyapatite layer because of the change in the surface morphology. This modification is even more appreciable by looking at the SEM images taken at higher magnification. The three samples display a compact surface composed of large plate-like structures fused together. For this reason, it was not necessary to perform the SEM analysis on the sample samples after 3 days of immersion into SBF. Whereas, the calcium nitrate samples sintered at 700

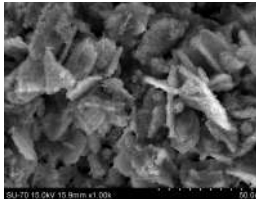
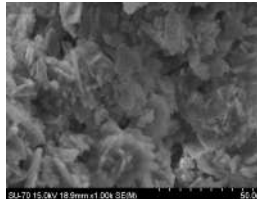
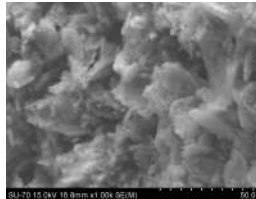
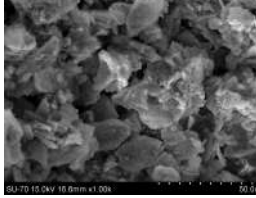
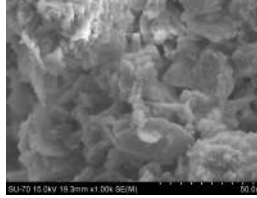
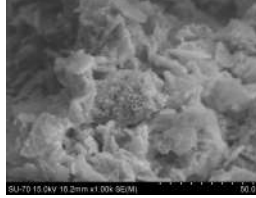
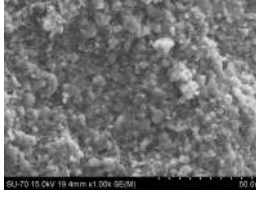
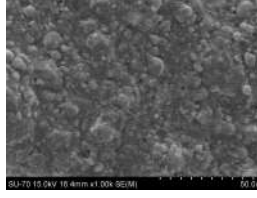
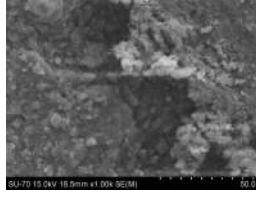
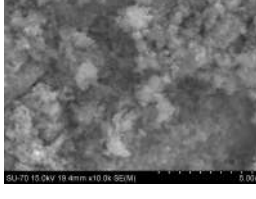
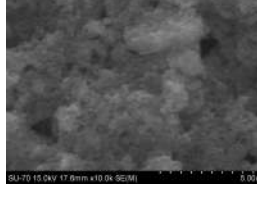
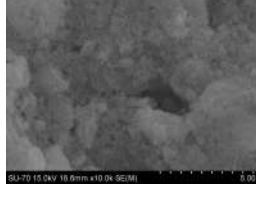
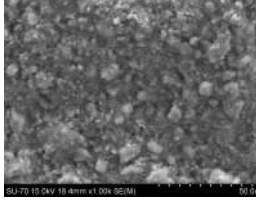
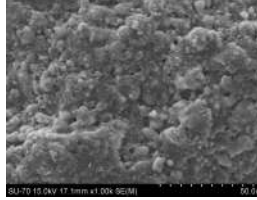
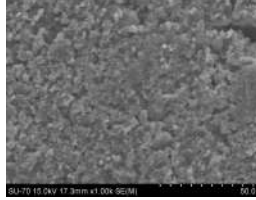
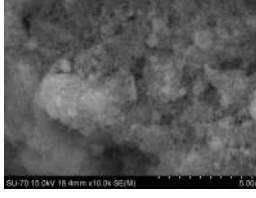
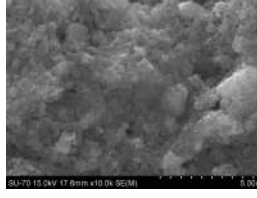

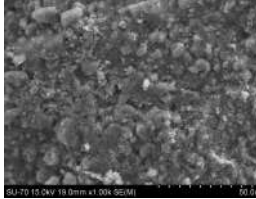
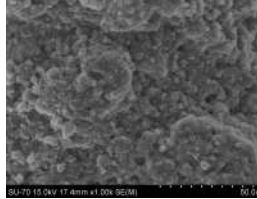
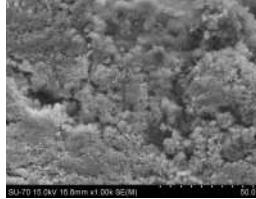
°C, after 1 day of soaking, seem to display a coverage layer formed by needle-like structures and small grains that increased their size after 3 days of immersion in order to form bigger plate-like crystals.

As previously said, the samples synthesized from calcium acetate displayed a surface composed of many large and well-defined plate-like crystal structures oriented in different directions. After their immersion in SBF, it is possible to notice the growth of the plate-like hydroxyapatite crystals that is driven by the thin deposited HAp film covering the starting surface (visible in the second image of Ac(3)-10%, 400 °C sample of *Table 12*). Meanwhile, the three scaffolds made of commercial hydroxyapatite, which possessed a more compact superficial surface, showed an enlargement of the flat plate-like aggregates after their soaking in SBF solution. By looking at these plate structures with a higher magnification power, it is possible to notice that they are formed by an assembly of grain-like crystals, which are constituted by smaller HAp particles. In general, for the scaffold samples, it seems that the novel hydroxyapatite particles prefer deposit and growth by taking the morphological structure of the original surface compared to the formation of needle-like crystals.

Sample name	SEM before incubation in SBF	SEM after 1 day in SBF	SEM after 3 day in SBF
Nit(3)-3%, 400 °C	 	 	/

<p>Nit(3)-5%, 400 °C</p>	 	 	<p>/</p>
<p>Nit(3)-10%, 400 °C</p>	 	 	<p>/</p>
<p>Nit(3)-3%, 700 °C</p>	 	 	 
<p>Nit(3)-5%, 700 °C</p>			

			
Nit(3)-10%, 700 °C	 	 	 
Ac(3)-3%, 400 °C			
Ac(3)-5%, 400 °C			
Ac(3)-10%, 400 °C			
Ac(3)-3%, 700 °C			

Ac(3)-5%, 700°C			
Ac(3)-10%, 700 °C			
Sc-3%, 700 °C			
			
Sc-5%, 700 °C			
			
Sc-10%, 700 °C			

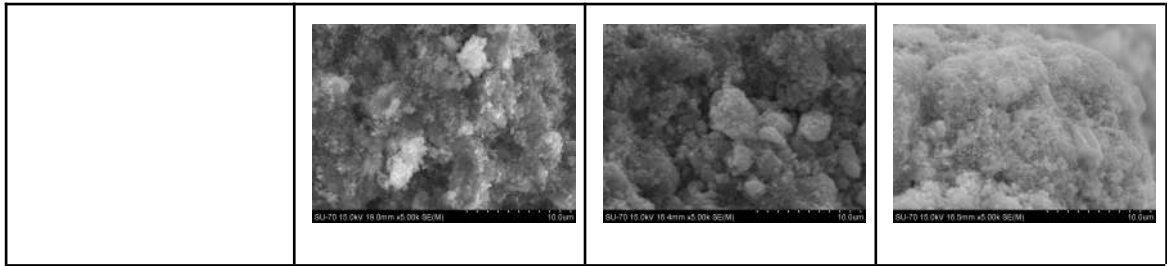


Table 12: SEM images of the several ceramic material and scaffold synthesized from calcium nitrate tetrahydrate, calcium acetate hydrate and commercial HAp, that where immersed in SBF and collected after 1 day and 3 days

5.5. Mechanical test

The uniaxial compression test is a fundamental materials science and engineering test that is used to determine the behavior or response of an isotropic material while it experiences a compressive load by measuring fundamental variables, such as strain, stress, and deformation. From these measurements, it is possible to determine different properties such as the maximum compressive strength, yield strength, ultimate strength, elastic limit, the Young's (elastic) modulus and Poisson's ratio. With the understanding of these different parameters and the values associated with a specific material it may be determined whether or not the material is suited for specific applications or if it will fail under the specified stresses.

The stress–strain curve of brittle materials in compression typically has an initial linear region followed by a region in which the shortening increases at a higher rate than does the load. The linear region is obtained due to the fact that the material during the compression behaves elastically up to a certain load. Meanwhile, the other region is obtained when the material fails suddenly by splitting or by cracking.

A series of images were taken while the uniaxial test was carried out in the direction perpendicular to the printing plane. Soon as the load begins to rise, some damages start to appear in the vicinity of the contact with the compression plates and this is noticeable due to the detachment of some small pieces from the main structure. However, being the damages localized, they do not compromise the structure's integrity (*Figure 13(a) and 13(b)*). At a certain load, many cracks develop perpendicularly to the horizontal plane that leads to the fragmentation of the structure into a bunch of irregular and disconnected

pillars (*Figure 13(c) and 13(d)*). After the complete failure of the scaffold's structure, the morphology of the sample is constituted by a mixture of bigger and irregular pieces and fine powder, which appears to have formed more at the points of contact between the material and the press (*Figure 13(e)*).

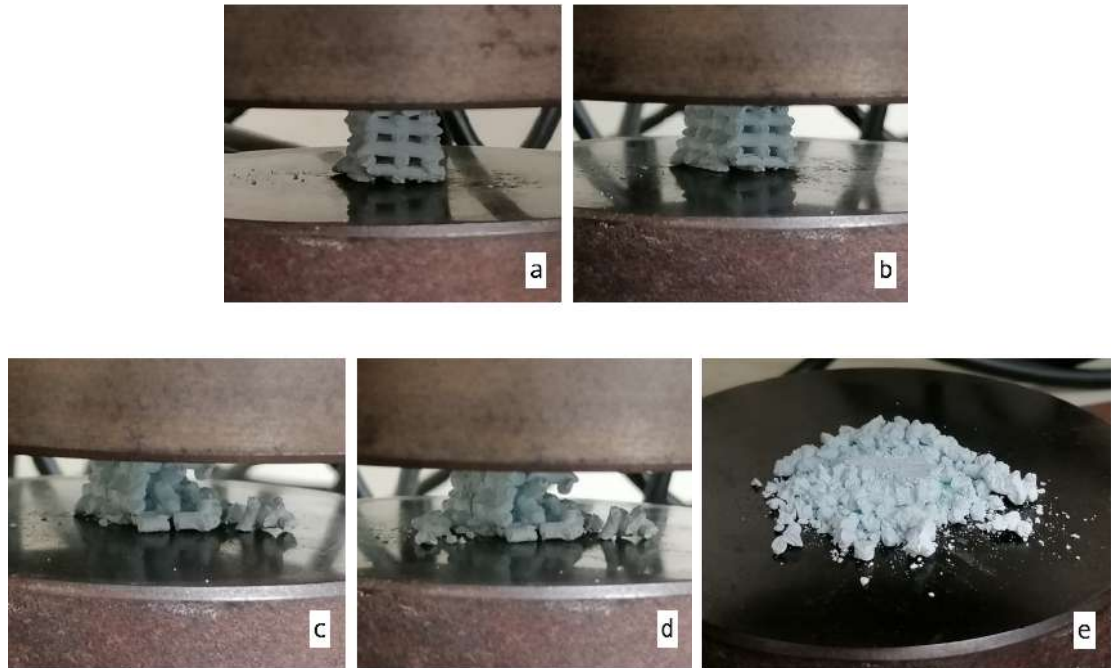
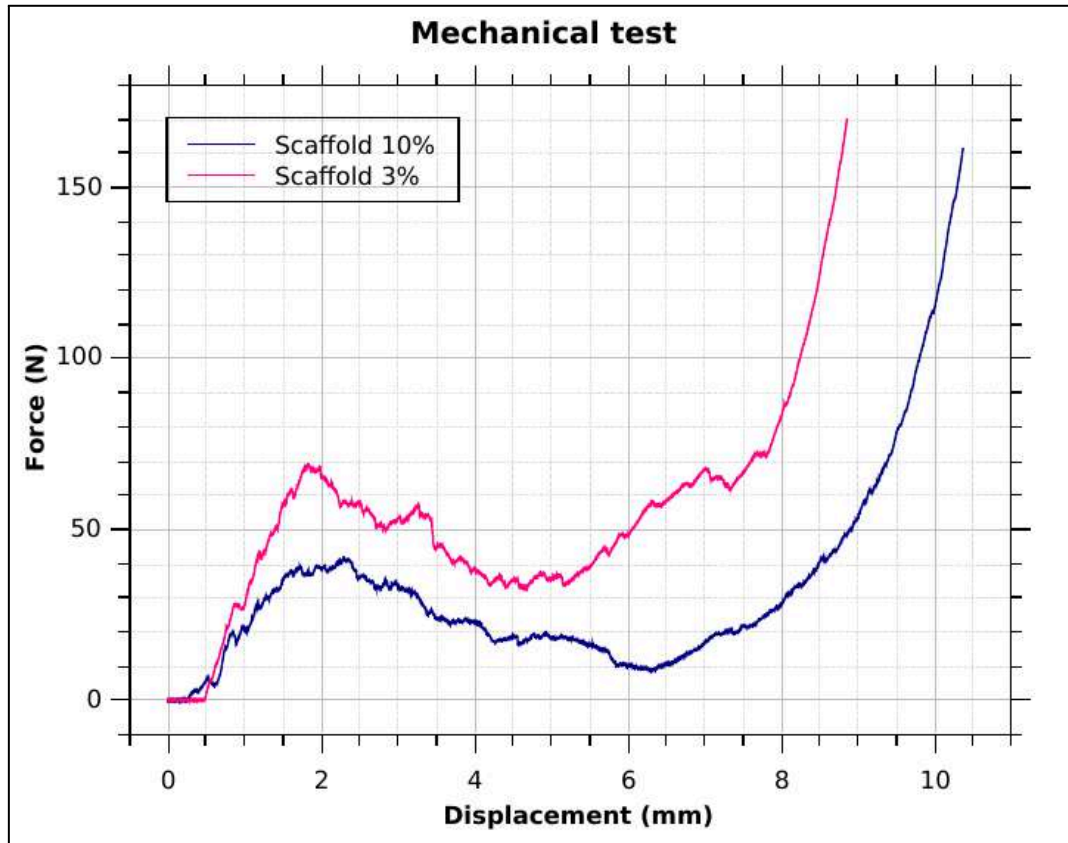


Figure 13: Images sequence captured during the uniaxial test performed in the orthogonal direction to the plane showing the evolution of the damage: (a and b) first contact damage appear from different angle of view, (c and d) failure of part of the structure at the later stage of test due to the multiple longitudinal cracks, and (e) final aspect of the scaffold at the end of the mechanical compressive stress.

By looking at the stress-strain curve (*Graph 4*), a significant drop in the load is observable for both the two scaffolds tested and this is associated with the appearance of the main longitudinal cracks. The onset of the first of these cracks usually corresponds to the maximum load, and therefore determines the compressive strength of the scaffolds. Some secondary fracture events are also detectable during the early stages of the compression test that are due to the formation of microcracks during the settling process, in which the scaffold begins to apply compressive strength against the surface of the press. After the maximum drop of load, the subsequent load decline is progressive,

indicating that the structure retains some significant mechanical resistance even after part of the structure crumbled.



Graph 4: Mechanical test performed on the scaffolds produced with commercial hydroxyapatite powder having 3% and 10% hydrogen peroxide

It is evident from these curves that the compressive strength of the HA scaffolds with 3% of hydrogen peroxide is clearly superior to that of the other structure synthesized with a higher percentage of H_2O_2 . This difference in compressive strength between the two samples is due to the fact that the stress is inversely proportional to the porosity of the material. For this reason, higher is the degree of porosity, which depends on the amount of H_2O_2 added, then lower will be the compressive stress of the scaffolds. Considering the maximum compressive stress of the scaffolds at 3% and 10% of H_2O_2 showed in *Table 13*, it is possible to suppose that the mechanical resistance of a scaffold with 5% of hydrogen peroxide, having the same size and structure, could falls between the maximum and minimum values obtained ($\sigma_{Sc-5\%} = 0.2-0.1 \text{ N/mm}^2 = 0.2-0.1 \text{ MPa}$).

Sample name	Section area (mm ²)	Maximum force applied (N)	Maximum compressive stress σ (N/mm ²)
Sc-3%, 700 °C	325.3	68.0	0.21
Sc-10%, 700 °C	401.1	41.5	0.10

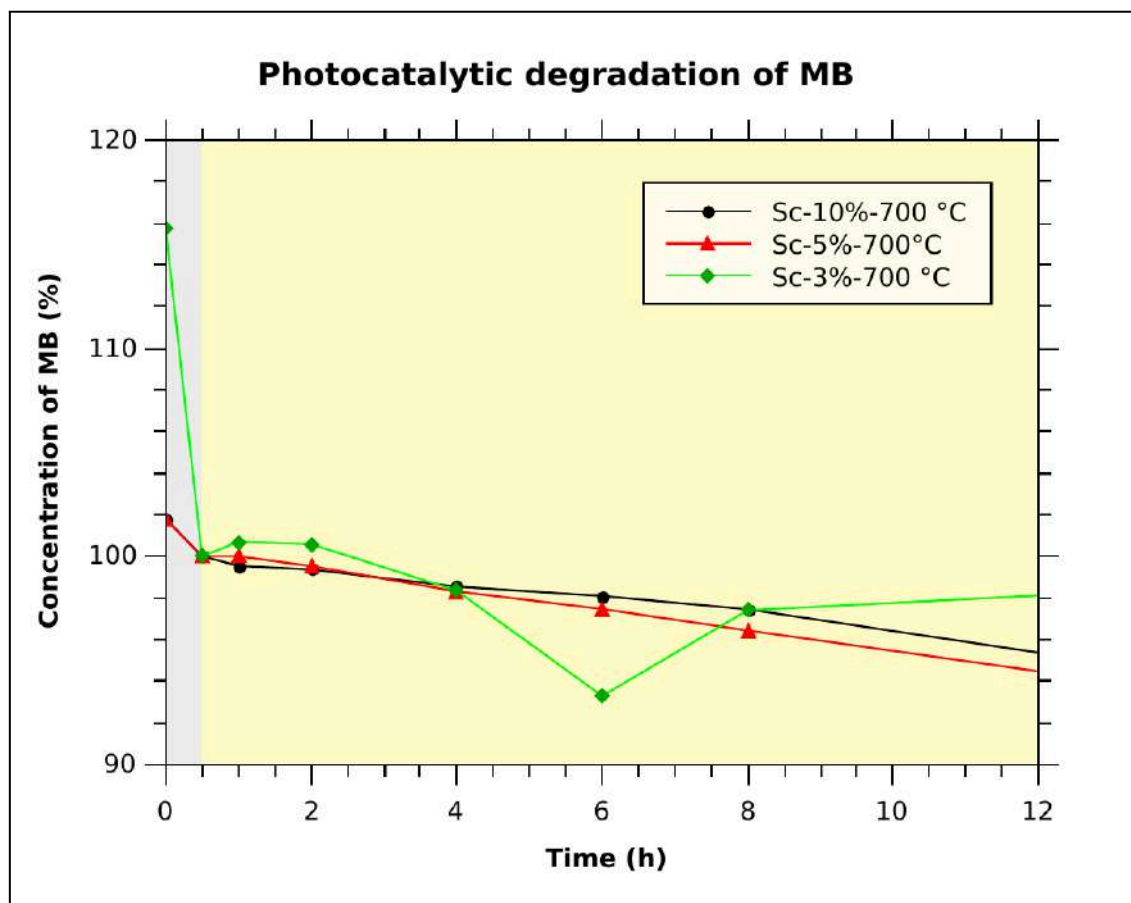
Table 13: Section area, maxim force applied and maximum compressive stress determined for the scaffold produced with commercial hydroxyapatite powder having 3% and 10% hydrogen peroxide

5.6. Photocatalytic test

Photocatalysis is an important catalytic method applied to photochemical reactions, that is carried out/accomplished with the aid of a catalyst that exerts its action when irradiated with light of appropriate wavelength. In particular, photocatalysts are semiconductor materials that possess a valence band (lower energy) and a conduction band (higher energy) that are separated by a forbidden band, or band gap, in which the electrons cannot be found. When the catalyst is irradiated with sufficient amount of energy light, which must be equal or greater than the band gap, a negatively charged electron of the valence band can absorb the photon and be promoted to the conduction band, leaving a positively charged hole in the valence band. These two charged species can react with molecules adsorbed on the surface of the material and such reactions can eventually lead to the degradation of these complex molecules, which may be harmful/hazardous to the human health and the environment, due to the formation of highly reactive oxygen species (free radicals).

It is known that an oxygen vacancy in the phosphate (PO_4) groups or a vacancy of an entire OH group in the HAp lattice, leads to a change in the forbidden energy band gap of the biomaterial, which assumes its typical pale-blue color. For this reason the photocatalytic activity of the three scaffolds synthesized with commercial hydroxyapatite powder, has been evaluated by measuring the degradation of methylene blue (MB), which functions as a photocatalyst sensitizer.

Considering the *Graph 5*, it is possible to notice that the scaffolds with 5% and 10% hydrogen peroxide slowly degraded the organic dye in presence of UVA-Vis light. It is possible to see that the concentration of MB starts to decrease already during the first hour of illumination of both the samples. Meanwhile, the scaffold produced with 3% of hydrogen peroxide starts to efficiently degrade the MB after the first two hours of illumination. It is possible to observe that after six hours the concentration of methylene blue decreased around 6-8% and then rose drastically. This can be explained by the fact that 4 mL of solution, corresponding to eight hours of illumination, were picked up the day after the start of the experiment. In particular, the solution was mixed in the dark for 30 minutes in order to resuspend the powder and after that the light was turned on. Maybe, during the night a greater amount of MB molecules desorbed from the sample surface and the sample wasn't able to rapidly oxidize them in presence of light, due to the fact that the degradation process seemed to be very slow at first. Another option could be that during the measurement of the absorbance with the spectrophotometer, the liquid picked up contained a high amount of suspended HAp particles, which interfered in the analysis.



Graph 5: Photocatalytic degradation of MB performed by the three scaffolds synthesized with commercial HAp powder with 3%, 5%, and 10% hydrogen peroxide, respectively

5.7. In vitro study: biocompatibility test

The MTT assay is a colorimetric assay for assessing cell metabolic activity. NAD(P)H-dependent oxidoreductase enzymes, largely located in the cytosolic compartment of the cells (mitochondria), are capable of reducing the tetrazolium yellow dye MTT into its insoluble formazan, which has a purple color (*Figure 14*). The amount of formazan produced is directly proportional to the number of living cells present in the culture and can be used to calculate cell viability. However, the MTT assay can also be used to measure cytotoxicity (loss of viable cells) or cytostatic activity (shift from proliferation to quiescence) of potential medicinal agents and toxic materials.

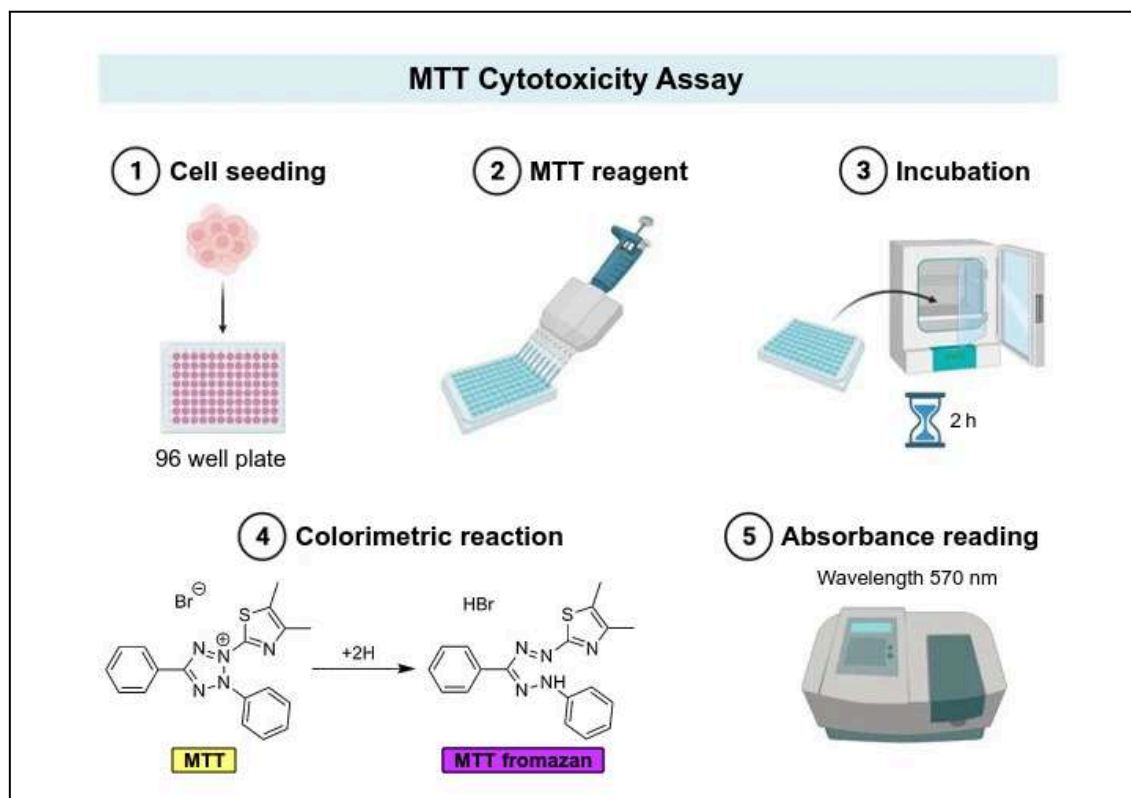


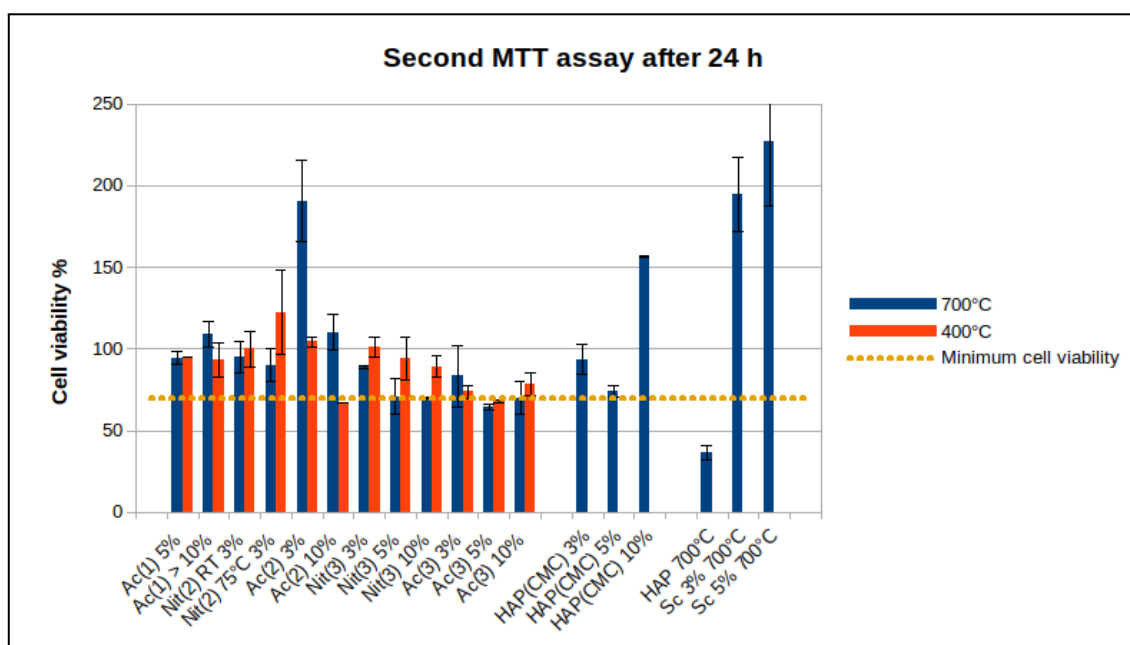
Figure 14: Schematic representation of the procedure for the MTT cytotoxicity assay

Therefore, the cytocompatibility of the hydroxyapatite (HA) materials was determined by performing the MTT assay on an osteosarcoma cell line (MG63). The rapidly dividing osteosarcoma tumor cells exhibit high rates of MTT reduction due to their increased metabolic activity. It is widely known that the degree of light absorption depends on the amount of formazan accumulated inside the cells and on their surface. For this reason, greater is the concentration of the purple dye then higher will be the absorbance.

The three tests performed were run in triplicate in order to obtain the medium value of cell viability after 24 h of incubation for each HAp sample. However, the first cell viability assay carried out did not obtain good results, therefore the HA samples were tested also without cells. The results obtained show the presence of some interference signals (high absorption) that are probably due to the presence of chemical residues, such as nitrates and acetate ions, attached to the ceramic and scaffold structures. As a result of this, the samples were washed to remove any ions present for the following tests.

Considering the other two cell viability assays (*Graph 6 and 7*), it is possible to notice that the content of viable cells is greater than 70% for most of the HA samples and this means that these materials can be used for biomedical applications. On the other hand, it is clearly visible that the scaffold synthesized with pure hydroxyapatite (HAp-700 °C) is highly cytotoxic. The reason for this is unclear at present, especially as the commercial HAp scaffolds with added H₂O₂ are highly biocompatible.

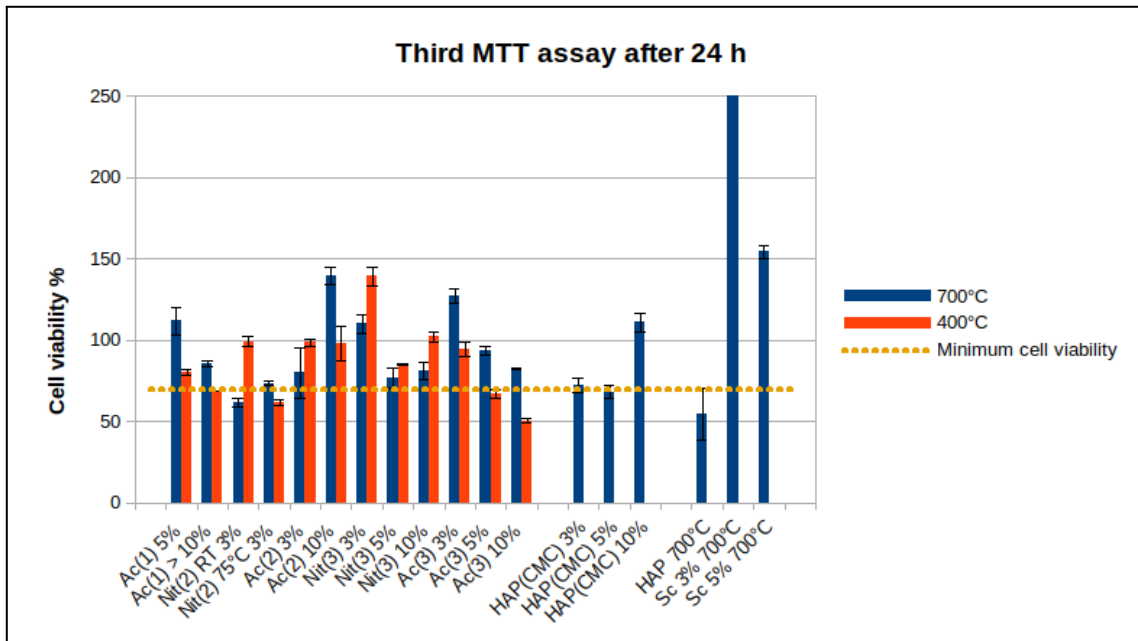
By looking at the second MTT assay, it is possible to observe that in general with the increase of the concentration of hydrogen peroxide, the cellular viability decreases for almost all the ceramic samples. Meanwhile, this tendency seems to be reversed for the scaffolds, with the only exception of the scaffold produced by adding 5% of H₂O₂ and the minimum amount of sodium carboxymethylcellulose (CMC).



Graph 6: Second MTT assay after 24 h of incubation with osteosarcoma cell line (MG63)

Regarding the third MTT assay (*Graph 7*), it is evident that the samples produced by using the HAp NPs obtained through the third sol-gel synthesis, Nit(3) and Ac(3), possess the same decreasing trend present also in *Graph 6*. However, the sample synthesized with calcium acetate and sintered at 700 °C showed a higher cell viability with respect to the samples sintered at a lower temperature (carbon residues) and the ones synthesized with

calcium nitrate. The cell viability of scaffolds produced with the addition of sodium carboxymethylcellulose is slightly decreased compared to the previous results. This is also true regarding the scaffolds produced by adding to the starting paste only 3% and 5% of hydrogen peroxide. Nevertheless, the scaffold having the lowest amount of H₂O₂ seems to be more biocompatible.



Graph 7: Second MTT assay after 24 h of incubation with osteosarcoma cell line (MG63)

Conclusions and Future works

In the first part of this work, the synthesis of HAp powder was performed by a rapid sol-gel process using calcium nitrate tetrahydrate or calcium acetate hydrate as starting precursors for calcium ions, and orthophosphoric acid as starting precursor for phosphate ions, in a Ca/P ratio of 1.67. In order to produce the ceramic samples, the hydroxyapatite powder produced was diluted with the minimum amount of water and reacted with different concentrations of hydrogen peroxide, which was used as pore-foaming agent. After giving them the shape of the semi-spherical disks, the samples were sintered at two different temperatures in order to study how their composition, morphology, mechanical properties, bioactivity and biocompatibility vary according to this parameter. In addition, porous scaffolds were synthesized with commercial hydroxyapatite which reacted with the same percentage of hydrogen peroxide used for ceramic materials. Some of these samples were produced by adding the minimum amount of sodium carboxymethylcellulose in order to increase the viscosity of the paste, while others were produced by creating a paste that has a HAp/solvent ratio of 1:1 in order to avoid the employment of additives.

In the second part of this thesis, the composition and the surface morphology were evaluated by performing X-Ray Diffraction (XRD), optical microscopy and Scanning Electron microscopy (SEM) techniques. It has been noticed that the choice of the starting calcium-precursor and the sintering temperature used greatly influenced the XRD patterns of the samples. In general, the pattern of the acetate samples sintered at lower temperature present broad peaks with low intensity values compared to the peaks of the equivalent nitrate samples. This is due to the fact that the crystalline structure of the HAp materials produced contains some unreacted acetate (carbon residues) that remains attached to their surface. The effect of the temperature and also the presence of carbon residues influence also the superficial morphology of the samples. From the optical images, it is possible to clearly see the difference in color of the acetate samples sintered at lower temperature (brown) and the ones at higher temperature (bright-white). The samples with nitrates assumed all the same color due to the fact that they do not contain carbon atoms. Meanwhile, the scaffold synthesized with only commercial hydroxyapatite powder and hydrogen peroxide assumed a light-blue color, which is due to the presence of oxygen vacancies in the hexagonal crystal lattice. The surface morphology of all the samples was investigated with SEM and it is possible to affirm that the wheel-define plate-like and needle-like crystalline structures, that are typical of HAp, were better achieved in the acetate samples sintered at a

higher temperature. The nitrate and scaffold samples obtained showed mainly a rough and compact surface formed by the aggregation of larger plate-like structures and grains.

The superficial surface area was evaluated by performing the BET analysis, while the pore radius was determined by applying the BJH method. From the data, it was possible to notice that most of the samples have similar SSA values. However, the sample synthesized with calcium acetate and sintered at lower temperature have SSA four/five times greater with respect to the other samples. This could be explained by the fact that the sample still contains some carbon that is well known to produce high SSA materials.

The biomineralization assay with SBF was performed in order to evaluate the bioactivity of the HAp ceramic materials and scaffolds. After their immersion in SBF, it is possible to notice the growth of the plate-like and needle-like hydroxyapatite crystals that is driven by the thin deposited HAp film covering the surface of the acetate samples. However, the SEM images also showed an enlargement of the grains and the flat plate-like aggregates present on the surface of both the nitrate samples and the scaffolds.

The characterization of the scaffolds proceeds with the assessment of their chemical properties, by evaluating their compressive strength. Both of the scaffolds tested have shown a very low compressive strength (far below the one in real bone), that could be explained by the fact that extruding the scaffold by hand didn't allowed the precise control of the flow of the paste from the extruder and the maintenance of the correct space distance between the filaments of each layer. A strategy to overcome this problem can be the production of these scaffolds by using the 3D-printing machine that was present in the research laboratory. However, it was not possible to use it because the three extruders available have a diameter that is too large compared to the size of the scaffolds designed.

Afterwards, the photocatalytic activity of the light-blue scaffolds was evaluated by studying the degradation of the methylene blue dye under UVA-Vis light irradiation. In general, the scaffolds showed a poor catalytic ability, since the degradation of MB was only around 94-96% during the entire 12 hours of testing. However, the aim of this work of thesis was to synthesize porous and strength ceramic materials and scaffolds, thus the results coming from the BET analysis and the uniaxial compression test are more valuable.

Lastly, the MTT assay, performed on MG63 cell line, validated the hypothesis that most of the samples are not cytotoxic after 24 hours of incubation meaning that HAp is a biomaterial that can support cell attachment and proliferation. However, further studies are necessary in order to understand the reason

behind the highly toxicity shown by the scaffold produced from pure commercial hydroxyapatite powder.

In conclusion, from this work it is possible to conclude that both ceramic materials and scaffolds produced with hydroxyapatite powder have obtained a good range of meso and microporosity, which allowed a good attachment and cell proliferation, making them ideal for biomedical applications. However, the compressive strength of the scaffolds is far below the one in real bone. Regarding this problem, further studies can be conducted in order to increase the Young's modulus and the maximum compressive strength. An example could be the synthesis of a HAp scaffold by robocasting or 3D-printing with the addition of copper ions or graphene or the creation of a composite material, like biphasic calcium phosphate.

Appendix A - Abbreviations

Ac: Acetate

AMPs: Antimicrobial Peptides

BCP: Biphasic Calcium Phosphate

BET: Brown, Emmet and Teller

BGs: Bioglasses

BGS: Bone Graft Substitutes

BJH: Barrett, Joyner and Helanda

BLC's: Bone Lining Cells

BMUs: Basic Multicellular Units

BMPs: Bone Morphogenetic Proteins

BMP-2: Bone Morphogenetic Protein-2

BSP: Bone Sialoprotein

CaP: Calcium Phosphate

CBFA1: Core Binding Factor Alpha-1

CCEF: Capacitively Coupled Electrical Field

CMC: Sodium Carboxymethylcellulose

DCP: Dicalcium Phosphate

DI: Deionized

DMSO: Dimethyl Sulfoxide

ECM: Extracellular Matrix

FGFs: Fibroblast Growth Factors

HA or HAp: Hydroxyapatite

IAFF: Infection After Fracture Fixation

IGFI: Insulin Growth Factor-I

IL-6: Interleukin-6

IUPAC: International Union of Pure and Applied Chemistry

LIPUS: Low-Intensity Pulsed Ultrasound

MB: Methylene Blue

MCP: Monocalcium phosphate
M-CSF: Monocyte/macrophage Colony Stimulating Factor
MTT: 3-(4,5-dimethylthiazol-2-yl)-2,5-diphenyltetrazolium bromide
Nit: Nitrate
NPs: Nanoparticles
OCN: Osteocalcin
OS: Osteosarcoma
PEMF: Pulsed Electromagnetic Field
PTH: Parathyroid Hormone
RANKL: Receptor Activation of NF- κ B Ligand
rER: rough-surfaced Endoplasmic Reticulum
SBF: Simulated Body Fluid
Sc: Scaffold made from commercial HAp powder
SEM: Scanning Electron Microscopy
SEs: Secondary Electrons
SSA: Specific Surface Area
TCP: Tricalcium Phosphate
TNF- α : Tumor Necrosis Factor- α
TGF- β : Transforming Growth Factor- β
UV: Ultraviolet
UVA: Ultraviolet-A
XRD: X-Ray Diffraction

References

- (1) Michael H. Ross H. Ross, W. P. *Histology: A Text and Atlas, with Correlated Cell and Molecular Biology*, 6th ed.; Lippincott Williams & Wilkins: 351 West Camden Street 2001 Market Street Baltimore, 2010.
- (2) Florencio-Silva, R.; Simões, M. J.; Cerri, P. S. Biology of Bone Tissue: Structure, Function, and Factors That Influence Bone Cells. *BioMed Res. Int.*
- (3) Franz-Odenaal, T. A.; Hall, B. K.; Witten, P. E. Buried Alive: How Osteoblasts Become Osteocytes. *Dev. Dyn.* **2006**, *235* (1), 176–190. <https://doi.org/10.1002/dvdy.20603>.
- (4) Rochefort, G. Y.; Pallu, S.; Benhamou, C. L. Osteocyte: The Unrecognized Side of Bone Tissue. *Osteoporos. Int.* **2010**, *21* (9), 1457–1469. <https://doi.org/10.1007/s00198-010-1194-5>.
- (5) Cao, W.; Helder, M. N.; Bravenboer, N.; Wu, G.; Jin, J.; Ten Bruggenkate, C. M.; Klein-Nulend, J.; Schulten, E. A. J. M. Is There a Governing Role of Osteocytes in Bone Tissue Regeneration? *Curr. Osteoporos. Rep.* **2020**, *18* (5), 541–550. <https://doi.org/10.1007/s11914-020-00610-6>.
- (6) Matic, I.; Matthews, B. G.; Wang, X.; Dymont, N. A.; Worthley, D. L.; Rowe, D. W.; Grcevic, D.; Kalajzic, I. Quiescent Bone Lining Cells Are a Major Source of Osteoblasts During Adulthood. *Stem Cells* **2016**, *34* (12), 2930–2942. <https://doi.org/10.1002/stem.2474>.
- (7) Boyce, B.; Yao, Z.; Xing, L. Osteoclasts Have Multiple Roles in Bone in Addition to Bone Resorption. *Crit. Rev. Eukaryot. Gene Expr.* **2009**, *19* (3), 171–180. <https://doi.org/10.1615/CritRevEukarGeneExpr.v19.i3.10>.
- (8) Zhu, W.; Li, C.; Yao, M.; Wang, X.; Wang, J.; Zhang, W.; Chen, W.; Lv, H. Advances in Osseointegration of Biomimetic Mineralized Collagen and Inorganic Metal Elements of Natural Bone for Bone Repair. *Regen. Biomater.* **2023**, *10*, rbad030. <https://doi.org/10.1093/rb/rbad030>.
- (9) Rosa, N.; Moura, M. F. S. F.; Olhero, S.; Simoes, R.; Magalhães, F. D.; Marques, A. T.; Ferreira, J. P. S.; Reis, A. R.; Carvalho, M.; Parente, M. Bone: An Outstanding Composite Material. *Appl. Sci.* **2022**, *12* (7), 3381. <https://doi.org/10.3390/app12073381>.
- (10) Ma, C.; Du, T.; Niu, X.; Fan, Y. Biomechanics and Mechanobiology of the Bone Matrix. *Bone Res.* **2022**, *10* (1), 59. <https://doi.org/10.1038/s41413-022-00223-y>.
- (11) Chang, B.; Liu, X. Osteon: Structure, Turnover, and Regeneration. *Tissue Eng. Part B Rev.* **2022**, *28* (2), 261–278. <https://doi.org/10.1089/ten.teb.2020.0322>.
- (12) Morgan, E. F.; Unnikrisnan, G. U.; Hussein, A. I. Bone Mechanical Properties in Healthy and Diseased

-
- States. *Annu. Rev. Biomed. Eng.* **2018**, *20* (1), 119–143.
<https://doi.org/10.1146/annurev-bioeng-062117-121139>.
- (13) Oftadeh, R.; Perez-Viloria, M.; Villa-Camacho, J. C.; Vaziri, A.; Nazarian, A. Biomechanics and Mechanobiology of Trabecular Bone: A Review. *J. Biomech. Eng.* **2015**, *137* (1), 010802.
<https://doi.org/10.1115/1.4029176>.
- (14) Hadjidakris, D. J.; Androulakis, I. I. Bone Remodeling. *Ann. N. Y. Acad. Sci.* **2006**, *1092* (1), 385–396.
<https://doi.org/10.1196/annals.1365.035>.
- (15) Raggatt, L. J.; Partridge, N. C. Cellular and Molecular Mechanisms of Bone Remodeling. *J. Biol. Chem.* **2010**, *285* (33), 25103–25108. <https://doi.org/10.1074/jbc.R109.041087>.
- (16) Capulli, M.; Paone, R.; Rucci, N. Osteoblast and Osteocyte: Games without Frontiers. *Arch. Biochem. Biophys.* **2014**, *561*, 3–12. <https://doi.org/10.1016/j.abb.2014.05.003>.
- (17) Dimitriou, R.; Jones, E.; McGonagle, D.; Giannoudis, P. V. Bone Regeneration: Current Concepts and Future Directions. *BMC Med.* **2011**, *9* (1), 66. <https://doi.org/10.1186/1741-7015-9-66>.
- (18) Einhorn, T. A.; Gerstenfeld, L. C. Fracture Healing: Mechanisms and Interventions. *Nat. Rev. Rheumatol.* **2015**, *11* (1), 45–54. <https://doi.org/10.1038/nrrheum.2014.164>.
- (19) Majidinia, M.; Sadeghpour, A.; Yousefi, B. The Roles of Signaling Pathways in Bone Repair and Regeneration. *J. Cell. Physiol.* **2018**, *233* (4), 2937–2948. <https://doi.org/10.1002/jcp.26042>.
- (20) Coughlan, T.; Dockery, F. Osteoporosis and Fracture Risk in Older People. *Clin. Med.* **2014**, *14* (2), 187–191. <https://doi.org/10.7861/clinmedicine.14-2-187>.
- (21) Ho-Shui-Ling, A.; Bolander, J.; Rustom, L. E.; Johnson, A. W.; Luyten, F. P.; Picart, C. Bone Regeneration Strategies: Engineered Scaffolds, Bioactive Molecules and Stem Cells Current Stage and Future Perspectives. *Biomaterials* **2018**, *180*, 143–162.
<https://doi.org/10.1016/j.biomaterials.2018.07.017>.
- (22) Tu, K. N.; Lie, J. D.; Wan, C. K. V.; Cameron, M.; Austel, A. G.; Nguyen, J. K.; Van, K.; Hyun, D. Osteoporosis: A Review of Treatment Options.
- (23) Massari, L.; Benazzo, F.; Falez, F.; Perugia, D.; Pietrogrande, L.; Setti, S.; Osti, R.; Vaienti, E.; Ruosi, C.; Cadossi, R. Biophysical Stimulation of Bone and Cartilage: State of the Art and Future Perspectives. *Int. Orthop.* **2019**, *43* (3), 539–551. <https://doi.org/10.1007/s00264-018-4274-3>.
- (24) Giannoudis, P. V.; Dinopoulos, H.; Tsiridis, E. Bone Substitutes: An Update. *Injury* **2005**, *36* (3), S20–S27. <https://doi.org/10.1016/j.injury.2005.07.029>.
- (25) Corre, I.; Verrecchia, F.; Crenn, V.; Redini, F.; Trichet, V. The Osteosarcoma Microenvironment: A
-

-
- Complex but Targetable Ecosystem. *Cells* **2020**, *9* (4), 976. <https://doi.org/10.3390/cells9040976>.
- (26)Luetke, A.; Meyers, P. A.; Lewis, I.; Juergens, H. Osteosarcoma Treatment – Where Do We Stand? A State of the Art Review. *Cancer Treat. Rev.* **2014**.
- (27)Rothzerg, E.; Xu, J.; Wood, D. Different Subtypes of Osteosarcoma: Histopathological Patterns and Clinical Behaviour. *J. Mol. Pathol.* **2023**, *4* (2), 99–108. <https://doi.org/10.3390/jmp4020011>.
- (28)Desai, S. S.; Jambhekar, N. A. Pathology of Ewing’s Sarcoma/PNET: Current Opinion and Emerging Concepts. *Indian J. Orthop.* **2010**, *44* (4), 363–368. <https://doi.org/10.4103/0019-5413.69304>.
- (29)Biswas, B.; Bakhshi, S. Management of Ewing Sarcoma Family of Tumors: Current Scenario and Unmet Need. *World J. Orthop.* **2016**, *7* (9), 527. <https://doi.org/10.5312/wjo.v7.i9.527>.
- (30)Gazendam, A.; Popovic, S.; Parasu, N.; Ghert, M. Chondrosarcoma: A Clinical Review. *J. Clin. Med.* **2023**, *12* (7), 2506. <https://doi.org/10.3390/jcm12072506>.
- (31)Riedel, R. F.; Larrier, N.; Dodd, L.; Kirsch, D.; Martinez, S.; Brigman, B. E. The Clinical Management of Chondrosarcoma. *Curr. Treat. Options Oncol.* **2009**, *10* (1–2), 94–106. <https://doi.org/10.1007/s11864-009-0088-2>.
- (32)Marini, F.; Giusti, F.; Iantomasi, T.; Brandi, M. L. Congenital Metabolic Bone Disorders as a Cause of Bone Fragility. *Int. J. Mol. Sci.* **2021**, *22* (19), 10281. <https://doi.org/10.3390/ijms221910281>.
- (33)Yang, Y.; Chu, L.; Yang, S.; Zhang, H.; Qin, L.; Guillaume, O.; Eglin, D.; Richards, R. G.; Tang, T. Dual-Functional 3D-Printed Composite Scaffold for Inhibiting Bacterial Infection and Promoting Bone Regeneration in Infected Bone Defect Models. *Acta Biomater.* **2018**, *79*, 265–275. <https://doi.org/10.1016/j.actbio.2018.08.015>.
- (34)Steinmetz, S.; Wernly, D.; Moerenhout, K.; Trampuz, A.; Borens, O. Infection after Fracture Fixation. *EFORT Open Rev.* **2019**, *4* (7), 468–475. <https://doi.org/10.1302/2058-5241.4.180093>.
- (35)Metsemakers, W. J.; Kuehl, R.; Moriarty, T. F.; Richards, R. G.; Verhofstad, M. H. J.; Borens, O.; Kates, S.; Morgenstern, M. Infection after Fracture Fixation: Current Surgical and Microbiological Concepts. *Injury* **2018**, *49* (3), 511–522. <https://doi.org/10.1016/j.injury.2016.09.019>.
- (36)Jorge, L. S. Osteomyelitis: A Current Challenge. *Braz J Infect Dis.*
- (37)Miron, R. J. Optimized Bone Grafting. *Periodontol.* **2000** **2023**, prd.12517. <https://doi.org/10.1111/prd.12517>.
- (38)Hasan, A.; Byambaa, B.; Morshed, M.; Cheikh, M. I.; Shakoor, R. A.; Mustafy, T.; Marei, H. E. Advances in Osteobiologic Materials for Bone Substitutes. *J. Tissue Eng. Regen. Med.* **2018**, *12* (6), 1448–1468. <https://doi.org/10.1002/term.2677>.
-

-
- (39)Bharadwaj, A. An Overview on Biomaterials and Its Applications in Medical Science. *IOP Conf. Ser. Mater. Sci. Eng.* **2021**, *1116* (1), 012178. <https://doi.org/10.1088/1757-899X/1116/1/012178>.
- (40)Du, X.; Fu, S.; Zhu, Y. 3D Printing of Ceramic-Based Scaffolds for Bone Tissue Engineering: An Overview. *J. Mater. Chem. B* **2018**, *6* (27), 4397–4412. <https://doi.org/10.1039/C8TB00677F>.
- (41)Gao, C.; Deng, Y.; Feng, P.; Mao, Z.; Li, P.; Yang, B.; Deng, J.; Cao, Y.; Shuai, C.; Peng, S. Current Progress in Bioactive Ceramic Scaffolds for Bone Repair and Regeneration. *Int. J. Mol. Sci.* **2014**, *15* (3), 4714–4732. <https://doi.org/10.3390/ijms15034714>.
- (42)El-Ghannam, A.; Ducheyne, P. Bioactive Ceramics. In *Comprehensive Biomaterials*; Elsevier, 2011; pp 157–179. <https://doi.org/10.1016/B978-0-08-055294-1.00021-0>.
- (43)Eliaz, N.; Metoki, N. Calcium Phosphate Bioceramics: A Review of Their History, Structure, Properties, Coating Technologies and Biomedical Applications. *Materials* **2017**, *10* (4), 334. <https://doi.org/10.3390/ma10040334>.
- (44)Krishani, M.; Shin, W. Y.; Suhaimi, H.; Sambudi, N. S. Development of Scaffolds from Bio-Based Natural Materials for Tissue Regeneration Applications: A Review. *Gels* **2023**, *9* (2), 100. <https://doi.org/10.3390/gels9020100>.
- (45)Lichte, P.; Pape, H. C.; Pufe, T.; Kobbe, P.; Fischer, H. Scaffolds for Bone Healing: Concepts, Materials and Evidence. *Injury* **2011**, *42* (6), 569–573. <https://doi.org/10.1016/j.injury.2011.03.033>.
- (46)Jeong, J.; Kim, J. H.; Shim, J. H.; Hwang, N. S.; Heo, C. Y. Bioactive Calcium Phosphate Materials and Applications in Bone Regeneration. *Biomater. Res.* **2019**, *23* (1), 4. <https://doi.org/10.1186/s40824-018-0149-3>.
- (47)Di Bello, C.; Bagnò, A. *Biomateriali. Dalla scienza dei materiali alle applicazioni cliniche*, Seconda.; Pàtron: Bologna, 2016.
- (48)Bhat, S.; Uthappa, U. T.; Altalhi, T.; Jung, H.-Y.; Kurkuri, M. D. Functionalized Porous Hydroxyapatite Scaffolds for Tissue Engineering Applications: A Focused Review. *ACS Biomater. Sci. Eng.* **2022**, *8* (10), 4039–4076. <https://doi.org/10.1021/acsbmaterials.1c00438>.
- (49)Bystrov, V. S.; Piccirillo, C.; Tobaldi, D. M.; Castro, P. M. L.; Coutinho, J.; Kopyl, S.; Pullar, R. C. Oxygen Vacancies, the Optical Band Gap (E_g) and Photocatalysis of Hydroxyapatite: Comparing Modelling with Measured Data. *Appl. Catal. B Environ.* **2016**, *196*, 100–107. <https://doi.org/10.1016/j.apcatb.2016.05.014>.
- (50)Costa, S. L. O.; Silva, P. F.; Carvalho, G. K. G.; Almeida, Y. B. A.; Braga, A. S. N. A Brief Review of Beta Tricalcium Phosphate (β -TCP) Doped with Metal Ions. *Am. J. Eng. Res.* **2021**.
-

-
- (51) Bouler, J. M.; Pilet, P.; Gauthier, O.; Verron, E. Biphasic Calcium Phosphate Ceramics for Bone Reconstruction: A Review of Biological Response. *Acta Biomater.* **2017**, *53*, 1–12. <https://doi.org/10.1016/j.actbio.2017.01.076>.
- (52) Ben-Arfa, B. A. E.; Salvado, I. M. M.; Ferreira, J. M. F.; Pullar, R. C. Novel Route for Rapid Sol-Gel Synthesis of Hydroxyapatite, Avoiding Ageing and Using Fast Drying with a 50-Fold to 200-Fold Reduction in Process Time. *Mater. Sci. Eng. C* **2017**, *70*, 796–804. <https://doi.org/10.1016/j.msec.2016.09.054>.
- (53) Maçon, A. L. B.; Kim, T. B.; Valliant, E. M.; Goetschius, K.; Brow, R. K.; Day, D. E.; Hoppe, A.; Boccaccini, A. R.; Kim, I. Y.; Ohtsuki, C.; Kokubo, T.; Osaka, A.; Vallet-Regí, M.; Arcos, D.; Fraile, L.; Salinas, A. J.; Teixeira, A. V.; Vueva, Y.; Almeida, R. M.; Miola, M.; Vitale-Brovarone, C.; Verné, E.; Höland, W.; Jones, J. R. A Unified in Vitro Evaluation for Apatite-Forming Ability of Bioactive Glasses and Their Variants. *J. Mater. Sci. Mater. Med.* **2015**, *26* (2), 115. <https://doi.org/10.1007/s10856-015-5403-9>.

Acknowledgements

This thesis would not have been possible without the guidance and the help of several people who in one way or another contributed and extended this valuable assistance in the preparation and completion of this study.

Firstly, I would like to thank my supervisor, Robert Carlyle Pullar, whose guidance, support, extended knowledge and availability have enabled me to conduct and efficiently complete this thesis work.

A special thanks also goes to my assistant supervisor, Paula Seabra, for giving me the opportunity to carry out part of the internship at her research laboratory in the University of Aveiro.

The conclusions of this thesis would have not been as compelling without the people I have collaborated with during my Erasmus program. In particular, I would like to thank Marinelia Capela and Ana Caetano for their infinite patience and availability in this short period of time. Further thanks extend to all the technicians of the Department of MAterials and Ceramic Engineering (DEMaC)-CICECO, for performing the XRD analysis and the uniaxial compressive mechanical test, and acquiring the SEM images of all my samples.

I would like to show my gratitude also to Alessandra Quarta and Alessia Nito at Istituto di Nanotecnologia CNR NANOTEC, Lecce, Italy, for performing the MTT assays.

Finally, I would like to dedicate this important and valuable goal to my family, which helped and supported me through my studies, my close friends and colleagues, the people with whom I have shared moments of joy and sadness, but despite everything have remained by my side in all of these years.